15

Dye-sensitized Solar Cells

Kohjiro Hara and Hironori Arakawa

National Institute of Advanced Industrial Science and Technology (AIST), Tsukuba, Japan

15.1 INTRODUCTION TO DYE-SENSITIZED SOLAR CELLS (DSSC)

15.1.1 Background

Photoelectrochemical solar cells (PSCs), consisting of a photoelectrode, a redox electrolyte, and a counter electrode, have been studied extensively. Several semiconductor materials, including single-crystal and polycrystal forms of *n*- and *p*-Si, *n*- and *p*-GaAs, *n*- and *p*-InP, and *n*-CdS, have been used as photoelectrodes. These materials, when used with a suitable redox electrolyte, can produce solar light-to-current conversion efficiency of approximately 10%. However, under irradiation, photocorrosion of the electrode in the electrolyte solution frequently occurs, resulting in poor stability of the cell, so efforts have been made worldwide to develop more stable PSCs.

Oxide semiconductor materials have good stability under irradiation in solution. However, stable oxide semiconductors cannot absorb visible light because they have relatively wide band gaps. Sensitization of wide band gap oxide semiconductor materials, such as TiO_2, ZnO, and SnO_2, with photosensitizers, such as organic dyes, that can absorb visible light has been extensively studied in relation to the development of photography technology since the late nineteenth century. In the sensitization process, photosensitizers adsorbed onto the semiconductor surface absorb visible light and excited electrons are injected into the conduction band of the semiconductor electrodes. Dye-sensitized oxide semiconductor photoelectrodes have been used for PSCs.

Gerischer and Tributsch studied a ZnO electrode sensitized by organic dyes including rose bengal, fluorescein, and rhodamine B [1, 2]. In early studies, however, single-crystal and polycrystal materials, which cannot adsorb a large amount of dye, were used for the photoelectrode, which resulted in low light-harvesting efficiency (LHE) and,

Handbook of Photovoltaic Science and Engineering. Edited by A. Luque and S. Hegedus
 ISBN: 0-471-49196-9

consequently, low photon-to-current conversion efficiencies. Additionally, the organic dyes that were used had a narrow absorption range in visible light, which also contributed to low solar cell performance. Thus, to improve light-harvesting efficiencies and cell performance, researchers used two approaches: developing photoelectrodes with larger surface areas that could adsorb large amount of dye and synthesizing dyes with broader absorption ranges. Significant improvements in the performance of a dye-sensitized solar cell (DSSC, or Grätzel cell) have been mainly due to the development of high-performance nanoporous TiO_2 thin-film electrodes that have a large surface area capable of adsorbing a large amount of photosensitizer, and due to the synthesis of new Ru complex photosensitizers capable of absorbing in the wide visible and near-IR region from 400 to 800 or 900 nm.

Ru bipyridyl complexes are suitable photosensitizers because the excited states of the complexes have long lifetimes and oxidized Ru(III) has long-term chemical stability. Therefore, Ru bipyridyl complexes have been studied intensively as photosensitizers for homogeneous photocatalytic reactions and dye-sensitization systems. An Ru bipyridyl complex, bis(2,2′-bipyridine)(2,2′-bipyridine-4,4′-dicarboxylate)ruthenium(II), having carboxyl groups as anchors to adsorb onto the semiconductor surface, was synthesized and single-crystal TiO_2 photoelectrodes sensitized by the Ru complex were studied in 1979 to 1980 [3, 4].

Recent drastic improvements in the performance of DSSC have been made by Grätzel and coworkers at the Swiss Federal Institute of Technology (EPFL). They achieved a solar energy efficiency, η, of 7 to 10% under AM1.5 irradiation using a DSSC consisting of a nanocrystalline TiO_2 thin-film electrode having a nanoporous structure with large surface area, a novel Ru bipyridyl complex, and an iodine redox electrolyte [5, 6]. They also developed a Ru terpyridine complex that absorbs in the near-IR region up to 900 nm as a photosensitizer for a nanocrystalline TiO_2 photoelectrode: the resulting cell obtained $\eta = 10.4\%$ under AM1.5 with a short-circuit photocurrent density, J_{SC}, of 20.5 mA cm^{-2}, an open-circuit voltage, V_{OC}, of 0.72 V, and a fill factor (*ff*) of 0.70 [7, 8].

The DSSC is an attractive and promising device for solar cell applications that have been intensively investigated worldwide, and its PV mechanism is well understood [9–18]. Recently, commercial applications of the DSSC have been under intensive investigation. The cost of commercially fabricating DSSCs is expected to be relatively low because the cells are made of low-cost materials and assembly is simple and easy. In this chapter, we describe the DSSC, including its structure, component materials, characteristics, working mechanism, preparation, and long-term stability, and discuss the improvement of its performance and commercial applications.

15.1.2 Structure and Materials

The schematic structure of the DSSC constructed by the Grätzel group is shown in Figure 15.1. The composition of the DSSC is described in this section.

15.1.2.1 Transparent conducting oxide-coated glass substrate

Transparent conducting oxide (TCO)-coated glass is used as the substrate for the TiO_2 photoelectrode. For high solar cell performance, the substrate must have low

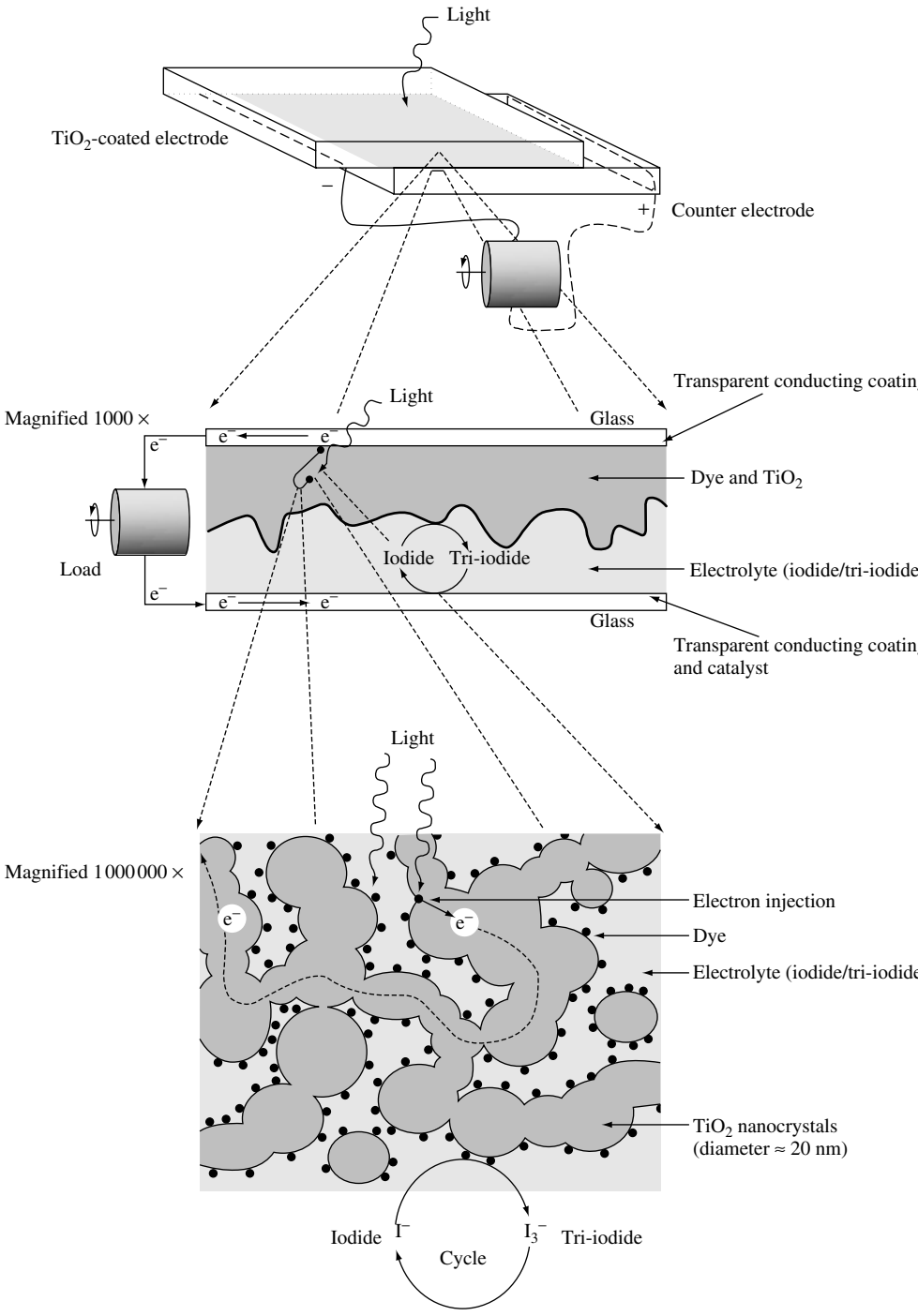

Figure 15.1 Schematic structure of the nanocrystalline dye-sensitized solar cell (DSSC). Reprinted from *Sol. Energy Mater. Sol. Cells*, **55**, Smestad G, 157–178, © 2002, with permission from Elsevier Science [15]

sheet resistance and high transparency. In addition, sheet resistance should be nearly independent of the temperature up to 500°C because sintering of the TiO_2 electrode is carried out at 450 to 500°C. Indium–tin oxide (ITO) is one of the most famous TCO materials. In spite of having low resistance at room temperature, ITO resistance increases significantly at high temperature in air. Usually, fluorine-doped SnO_2 is used as the TCO substrate for DSSCs (e.g. Nippon Sheet Glass Co., $R = 8–10\ \Omega$/square).

15.1.2.2 TiO_2 photoelectrode

Photoelectrodes made of such materials as Si, GaAs, InP, and CdS decompose under irradiation in solution owing to photocorrosion. In contrast, oxide semiconductor materials, especially TiO_2, have good chemical stability under visible irradiation in solution; additionally, they are nontoxic and inexpensive. The TiO_2 thin-film photoelectrode is prepared by a very simple process. TiO_2 colloidal solution (or paste) is coated on a TCO substrate and then sintered at 450 to 500°C, producing a TiO_2 film about 10 μm in thickness. Because this film is composed of TiO_2 nanoparticles (10–30 nm), giving it a nanoporous structure, the actual surface area of TiO_2 compared to its apparent surface area, roughness factor (rf), is >1000; that is, a 1-cm^2 TiO_2 film (10 μm thickness) has an actual surface area of 1000 cm^2. The dye is considered to be adsorbed on the TiO_2 surface in a monolayer. Thus, if the nanoporous TiO_2 film has a high rf, the amount of dye adsorbed is drastically increased (on the order of 10^{-7} mol cm^{-2}), resulting in an increase of LHE that is near 100% at the peak absorption wavelength of the dye. In comparison, the amount of adsorbed dyes on the surface of single-crystal and polycrystal materials is quite small, with only 1% LHE even at the peak wavelength.

Normally, the TiO_2 film contains large TiO_2 particles (250–300 nm), which can scatter incident photons effectively, to improve the LHE as shown later. The porosity of the film is also important because the electrolyte, which contains the redox ions, must be able to penetrate the film effectively to suppress the rate-determining step via diffusion of redox ions into the film. Appropriate porosity, 50 to 70%, is controlled in the sintering process by the addition of a polymer such as polyethylene glycol (PEG) and ethyl cellulose (EC) into the TiO_2 colloidal solution or paste. Figure 15.2 shows a scanning electron microscope (SEM) photograph of a typical nanocrystalline TiO_2 film. A detailed description of the procedure for preparing the TiO_2 film is given in Section 15.2.2.

15.1.2.3 Ru complex photosensitizer

The Ru complex photosensitizer, which contributes the primary steps of photon absorption and the consequent electron injection, is adsorbed onto the TiO_2 surface. The chemical structure of typical Ru complex photosensitizers developed by Grätzel's group are shown in Figure 15.3 (TBA is tetrabutylammonium cation, $(C_4H_9)_4N^+$), and Figure 15.4 shows absorption properties of the complexes in solution. The *y*-axis is represented by absorbance (A) and $1 - T(= 1 - 10^{-A})$, where T is the transmittance. The *cis*-bis(4,4′-dicarboxy-2,2′-bipyridine)dithiocyanato ruthenium(II) ($RuL_2(NCS)_2$ complex), which is referred to as N3 dye (or red dye), can absorb over a wide range of the visible regions from 400 to 800 nm. The trithiocyanato 4,4′4″-tricarboxy-2,2′:6′,2″-terpyridine ruthenium(II) (black dye) (RuL'$(NCS)_3$ complex), absorbs in the near-IR region up to

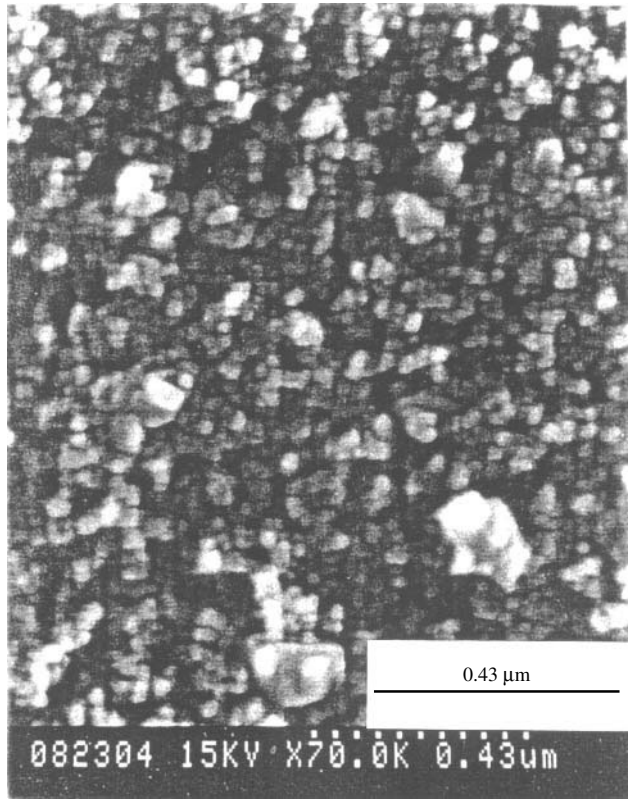

Figure 15.2 Scanning electron microscope photograph of a typical nanocrystalline TiO_2 film: the scale bar corresponds to 0.43 μm

900 nm. Absorption by these dyes in the visible and near-IR regions is attributed to the metal-to-ligand charge-transfer (MLCT) transition. The highest occupied molecular orbital (HOMO) and the lowest unoccupied molecular orbital (LUMO) are mainly derived from the d-orbitals of the Ru metal and the π^* orbital of the ligand, respectively. The NCS ligand shifts the HOMO level negatively, leading to a red shift in the absorption property of the complex, and also contributes electron acceptance from reduced redox ions (I^-). These Ru complexes have carboxyl groups to anchor to the TiO_2 surface. Anchoring causes a large electronic interaction between the ligand and the conduction band of TiO_2, resulting in effective electron injection from the Ru complex into the TiO_2. The Ru complex is adsorbed on the TiO_2 surface via either carboxylate bidentate coordination or ester bonding ($-C(=O)O-$) as measured by FT–IR absorption analysis [19–23]. Figure 15.5 shows the anchoring structure of the N3 dye adsorbed on the (101) surface of TiO_2. The coverage of the TiO_2 surface with the N3 dye reaches near 100% as derived from the surface area of TiO_2 and the amount of the dye.

15.1.2.4 Redox electrolyte

The electrolyte used in the DSSC contains I^-/I_3^- redox ions, which mediate electrons between the TiO_2 photoelectrode and the counter electrode. Mixtures of iodides such as

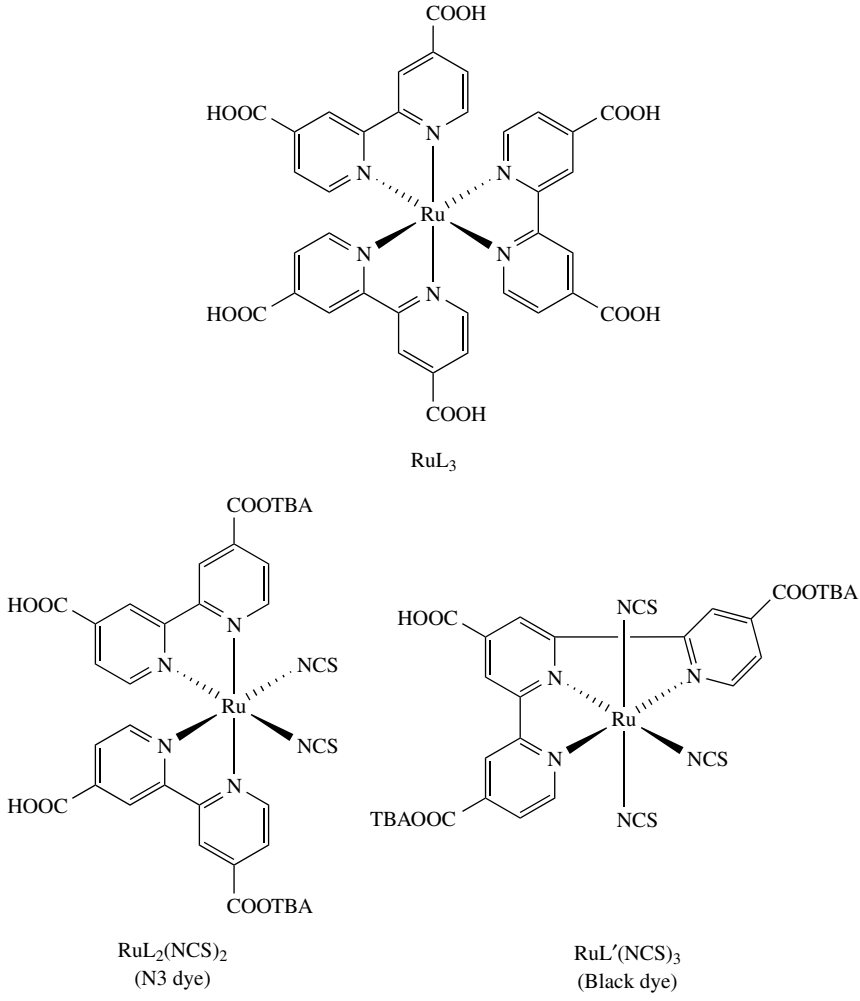

Figure 15.3 Molecular structures of typical Ru complex photosensitizers

LiI, NaI, KI, tetraalkylammonium iodide (R_4NI), and imidazolium-derivative iodides with concentrations of 0.1 to 0.5 M (M: molar concentration) and 0.05 to 0.1 M I_2 dissolved in nonprotonic solvents (e.g. acetonitrile, propionitrile, methoxyacetonitrile, propylene carbonate, and their mixture) are employed. Cell performance of DSSCs depends on counter cations of iodides such as Li^+, Na^+, K^+, and R_4N^+ owing to different ion conductivity in the electrolyte or adsorption on the TiO_2 surface, leading to a shift of the conduction-band level of the TiO_2 electrode [24, 25]. Viscosity of solvents directly affects ion conductivity in the electrolyte, and consequently the cell performance. To improve cell performance, low-viscosity solvents are desired. The diffusion coefficient of I_3^- in methoxyacetonitrile is estimated as $5.4–6.2 \times 10^{-6}$ $cm^2\,s^{-1}$ [24]. Basic compounds such as *tert*-butylpyridine are added to the electrolyte solution to improve cell performance, as shown later [6]. Br^-/Br_2 and hydroquinone have also been used as redox electrolyte for DSSC [25, 26], but the iodine redox electrolyte gives the best performance.

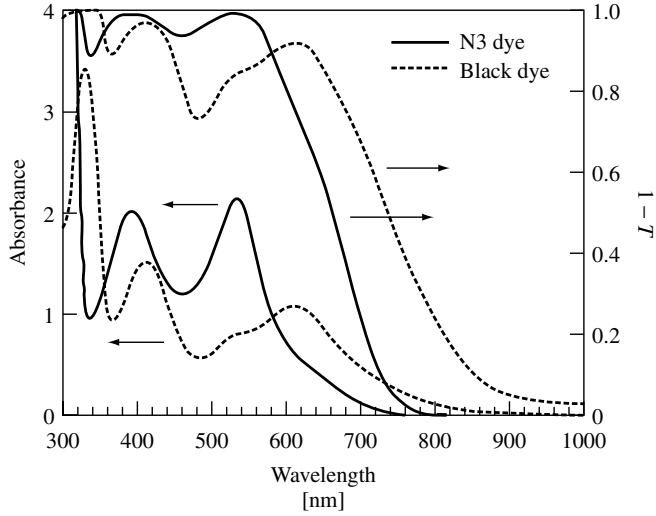

Figure 15.4 Absorption spectra of N3 dye and black dye represented by absorbance and light-harvesting efficiency, $1-T$ (T: transmittance): (——) N3 dye, (– – –) black dye

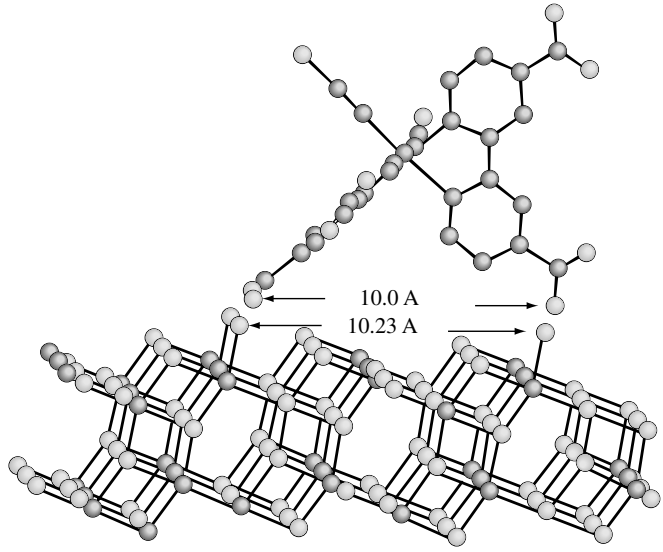

Figure 15.5 Anchoring structure of N3 dye adsorbed on the (101) surface of TiO_2: the top is N3 dye and the bottom is TiO_2. Reprinted with permission from © (2002) American Chemical Society

15.1.2.5 Counter electrode

Tri-iodide ions, I_3^-, formed by the reduction of dye cations with I^- ion, are re-reduced to I^- ions at the counter electrode. To reduce the tri-iodide ions, the counter electrode must have high electrocatalytic activity. Pt coated on TCO substrate (5–10 $\mu g\,cm^{-2}$ or approximately 200-nm thickness) or carbon are usually used as the counter electrode.

15.1.2.6 Sealing materials

A sealing material is needed to prevent the leakage of the electrolyte and the evaporation of the solvent. Chemical and photochemical stability of the sealing material against the electrolyte component, iodine, and the solvent is required. Surlyn (Du Pont), a copolymer of ethylene and acrylic acid, meets these requirements.

15.1.3 Mechanism

This section describes the primary processes that occur in a DSSC and discusses the solar energy–to–current conversion efficiencies of cells.

15.1.3.1 Primary processes

Figure 15.6 is a schematic energy diagram of a DSSC. The following primary steps convert photons to current:

1. Ru complex photosensitizers adsorbed on the TiO_2 surface absorb incident photon flux.
2. The photosensitizers are excited from the ground state (S) to the excited state (S^*) owing to the MLCT transition. The excited electrons are injected into the conduction band of the TiO_2 electrode, resulting in the oxidation of the photosensitizer.

$$S + h\nu \rightarrow S^* \quad [1]$$

$$S^* \rightarrow S^+ + e^-(TiO_2) \quad [2]$$

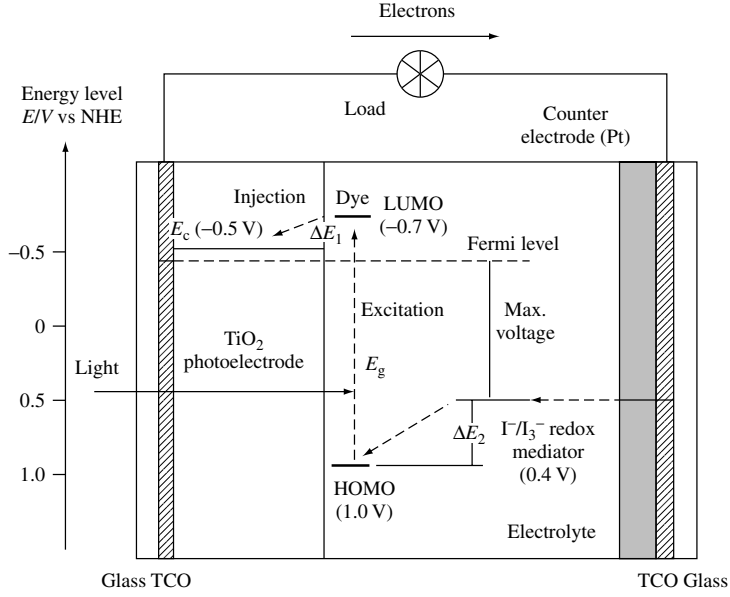

Figure 15.6 Schematic energy diagram and operating principle of DSSC

3. Injected electrons in the conduction band of TiO_2 are transported between TiO_2 nanoparticles with diffusion toward the back contact (TCO) and consequently reach the counter electrode through the external load and wiring.
4. The oxidized photosensitizer (S^+) accepts electrons from the I^- ion redox mediator, regenerating the ground state (S), and I^- is oxidized to the oxidized state, I_3^-.

$$S^+ + e^- \rightarrow S \quad [3]$$

5. The oxidized redox mediator, I_3^-, diffuses toward the counter electrode and is re-reduced to I^- ions.

$$I_3^- + 2e^- \rightarrow 3I^- \quad [4]$$

Overall, electric power is generated without permanent chemical transformation.

The performance of a DSSC is predominantly based on four energy levels of the component: the excited state (approximately LUMO) and the ground state (HOMO) of the photosensitizer, the Fermi level of the TiO_2 electrode, which is located near the conduction-band level, and the redox potential of the mediator (I^-/I_3^-) in the electrolyte. The photocurrent obtained from a DSSC is determined by the energy difference between the HOMO and the LUMO of the photosensitizer, analogous to the band gap, E_g, for inorganic semiconductor materials. The smaller the HOMO–LUMO energy gap, the larger the photocurrent will be because of the utilization of the long-wavelength region in the solar spectrum. The energy gap between the LUMO level and the conduction-band level of TiO_2, ΔE_1, is important, and the energy level of the LUMO must be sufficiently negative with respect to the conduction band of TiO_2 to inject electrons effectively. In addition, substantial electronic coupling between the LUMO and the conduction band of TiO_2 also leads to effective electron injection. The HOMO level of the complex must be sufficiently more positive than the redox potential of the I^-/I_3^- redox mediator to accept electrons effectively (ΔE_2). The energy gaps, ΔE_1 and ΔE_2, must be larger than approximately 200 mV as driving force for each of the electron-transfer reactions to take place with optimal efficiency [16].

In the case of solid–liquid junction solar cells, PSCs, the voltage is attributed to the energy gap between the Fermi level (near conduction-band level for *n*-type semiconductor) of the semiconductor electrode and the redox potential of the mediator in the electrolyte. As shown in Figure 15.6, the voltage in the DSSC is developed by the energy gap between the Fermi level of a TiO_2 electrode and the redox potential of the I^-/I_3^- in the electrolyte. The conduction-band level of the TiO_2 electrode and the redox potential of I^-/I_3^- were estimated to be -0.5 V versus normal hydrogen electrode (NHE) and 0.4 V versus NHE, respectively, as shown in Figure 15.6 [18] (or -0.7 V versus saturated calomel electrode (SCE) and 0.2 V versus SCE, respectively [12, 16]). Thus, in the case of a DSSC using a TiO_2 electrode and I^-/I_3^- redox mediator, the maximum voltage is expected to be approximately 0.9 V, depending on the electrolyte component because the Fermi level of the TiO_2 electrode depends on the electrolyte components and their concentrations.

In contrast to a conventional *p-n*-type solar cell, the mechanism of a DSSC does not involve a charge-recombination process between electrons and holes because electrons are only injected from the photosensitizer into the semiconductor and a hole is not formed in the valence band of the semiconductor. In addition, charge transport

takes place in the TiO_2 film, which is separated from the photon absorption site (i.e. the photosensitizer); thus, effective charge separation is expected. This photon-to-current conversion mechanism in a DSSC is similar to the mechanism for photosynthesis in nature, in which chlorophyll functions as the photosensitizer and charge transport occurs in the membrane.

In conventional *p-n*-type solar cells and classical PSCs using polycrystal or single-crystal photoelectrodes, electronic contact between the components that form the photovoltaically active junction, and the equilibrium between the electronic charge carriers in them, leads to space charge formation. Photogenerated charges are separated by the electric field in the space charge layer. In DSSC, however, the individual particle size is too small to form a space charge layer. Charge separation in DSSC has been discussed relative to an electrical field at the electrolyte/semiconductor interface, although not one due to space charge in the semiconductor [27]. Small cations, such as Li^+, in the electrolyte and H^+ released from the dyes upon binding, can adsorb (or intercalate) on the semiconductor surface. A dipole is formed across the Helmholtz layer between these cations and negatively charged species (iodide ions and the dye). The electrical potential drop across the Helmholtz layer will help separate the charges and reduce recombination with the dye cations or the redox mediator. Under illumination, this potential will decrease, as the electrons injected in the semiconductor will neutralize some of the positive charge at the surface.

15.1.3.2 Photovoltaic performance

Figure 15.7 shows the external spectral response curve of the photocurrent for nanocrystalline TiO_2 solar cells sensitized by N3 and black dyes with an I^-/I_3^- redox electrolyte, where the incident photon-to-current conversion efficiency (IPCE) is represented as a

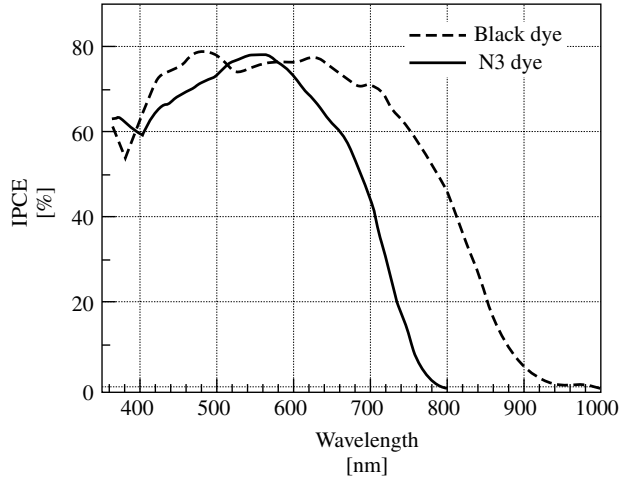

Figure 15.7 Spectral response curve of the photocurrent for the DSSC sensitized by N3 and black dyes: (——) N3 dye, (– – –) black dye. The incident photon-to-current conversion efficiency (IPCE) is plotted as a function of wavelength. The data is used from Reference [18]

function of wavelength. IPCE is obtained by the following equation:

$$\text{IPCE}[\%] = \frac{1240[\text{eV} \cdot \text{nm}] \times J_{\text{SC}}[\mu\text{A cm}^{-2}]}{\lambda[\text{nm}] \times \Phi[\mu\text{W cm}^{-2}]} \times 100 \tag{15.1}$$

where J_{SC} is the short-circuit photocurrent density for monochromatic irradiation, λ is the wavelength, and Φ is the monochromatic light intensity. As shown in Figure 15.7, solar cells sensitized by the Ru complex photosensitizers can efficiently convert visible light to current. N3 dye ($RuL_2(NCS)_2$) responds to light from 400 to 800 nm, and black dye ($RuL'(NCS)_3$) responds to the near-IR region up to 950 nm. The IPCE of the N3 dye-sensitized solar cell reaches 80% at 550 nm and exceeds 70% in the region from 400 to 650 nm. Taking into consideration losses due to light reflection and absorption by the TCO substrate, the internal photon-to-current conversion efficiency is effectively 90 to 100%, indicating high performance of the DSSC. IPCE is also given by the following equation:

$$\text{IPCE} = \text{LHE}\ \phi_{\text{inj}}\eta_{\text{c}} \tag{15.2}$$

$$\text{LHE} = 1 - T = 1 - 10^{-A} \tag{15.3}$$

where LHE is the light-harvesting efficiency, ϕ_{inj} is the quantum yield of electron injection, and η_{c} is the efficiency of collecting the injected electrons at the back contact. According to equation (15.2), if ϕ_{inj} and η_{c} are almost equal to unity, IPCE is determined by the LHE (i.e. $1 - T$) of the dye adsorbed on the film (shown in Figure 15.4).

Solar energy–to–electricity conversion efficiency, η, under white light irradiation (e.g. AM1.5) can be obtained by the following equation:

$$\eta = J_{\text{SC}} \times V_{\text{OC}} \times ff / I_0 \times 100 \tag{15.4}$$

where I_0 is the photon flux (approximately 100 mW cm^{-2} for AM1.5). A current versus voltage curve obtained for a nanocrystalline TiO_2 solar cell sensitized by black dye is shown in Figure 15.8. Evaluation of the performance was carried out at the National Renewable Energy Laboratory (NREL) operated by the US Department of Energy. An efficiency of 10.4% was obtained (cell size = 0.186 cm^2, $J_{\text{SC}} = 20.53$ mA cm^{-2}, $V_{\text{OC}} =$ 0.721 V, and $ff = 0.704$) [8, 18].

15.1.4 Charge-transfer Kinetics

15.1.4.1 Electron injection process

Recently, the electron-transfer kinetics in the DSSC, shown as a schematic diagram in Figure 15.9, have been under intensive investigation. Time-resolved laser spectroscopy measurements are used to study one of the most important primary processes, electron injection from photosensitizers into the conduction band of semiconductors [28–47]. The electron-transfer rate from the photosensitizer into the semiconductor depends largely on the configuration of the adsorbed photosensitizer material on the semiconductor surface and the energy gap between the LUMO level of the photosensitizer and the conduction-band

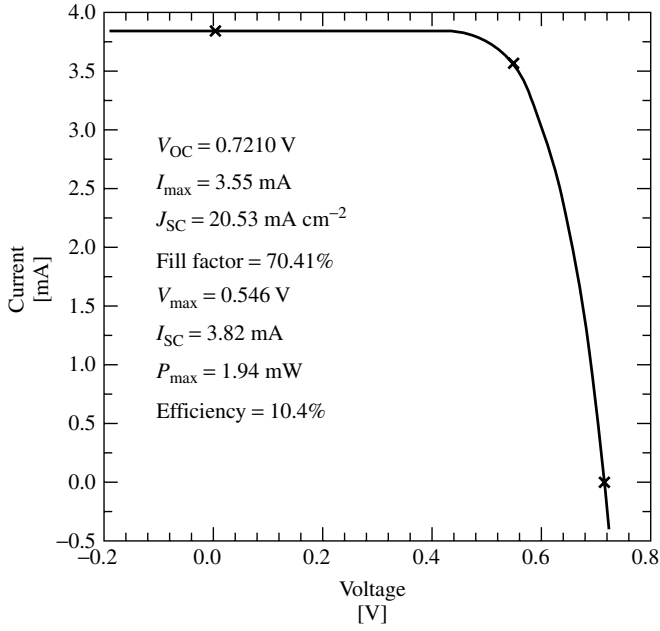

Figure 15.8 Photocurrent–voltage curve obtained for a nanocrystalline TiO_2 solar cell sensitized by black dye. The certified results were obtained at NREL (USA). Reprinted with permission from Hagfeldt A, Grätzel M, *Acc. Chem. Res.* **33**, 269–277 (2000). © (2002) American Chemical Society

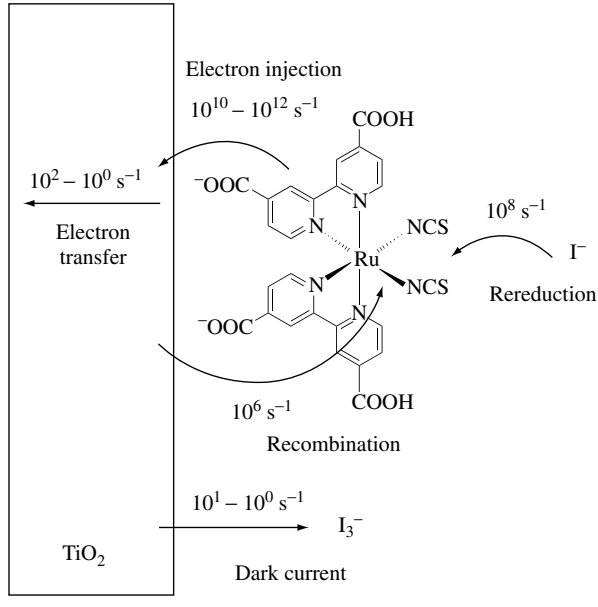

Figure 15.9 Schematic diagram of electron-transfer processes in DSSC

level of the semiconductor. For example, the rate constant for electron injection, k_{inj}, is given by Fermi's golden rule expression

$$k_{inj} = \left(\frac{4\pi^2}{h}\right)|V|^2\rho(E) \tag{15.5}$$

where V is the electronic coupling between the photosensitizer and the semiconductor, $\rho(E)$ is the density-of-states of the conduction band, and h is the Planck constant. The value of V is attributed to overlap between the wavefunction of the excited states of the photosensitizer and the conduction band, and it depends largely on the distance between the adsorbed photosensitizer material and the semiconductor surface. In a DSSC, the photosensitizer is strongly adsorbed on the semiconductor surface with carboxyl groups as the anchor, resulting in a very large V between the π^* orbital of the excited state of the photosensitizer and the conduction band of TiO_2, which consists of the unoccupied 3d orbital of Ti^{4+}. In addition, the conduction band of the semiconductor has a continuous and relatively large density-of-states. Thus, electron injection from the photosensitizer to the semiconductor occurs at a higher rate than does the relaxation from the excited state to the ground state (i.e. relaxation via the emission lifetime). For example, it has been observed that electron injection from N3 dye into TiO_2 occurs on the order of femtoseconds as measured by the time-resolved laser spectroscopy [28, 32]. This ultrafast rate of electron injection contributes to the high energy-conversion efficiencies of the DSSC.

In addition, the rate constant for electron injection depends largely on the semiconductor materials employed. A slower electron injection rate was observed with coumarin dyes and N3 dye injected into ZnO compared to the TiO_2 system [35, 37, 45]. The different rate constant may be caused by the difference in the electronic coupling between the π^* orbital of the dye and the accepting orbitals in ZnO and TiO_2 and/or their density-of-states. The states near the conduction-band edge of ZnO consist of the 4s orbitals of Zn^{2+}, while those of TiO_2 consist of the 3d orbitals of Ti^{4+}, which may result in the observed difference in their electronic coupling with the π^* orbital of the dye.

15.1.4.2 Charge recombination

The charge-recombination process (Figure 15.9) between injected electrons and oxidized dyes must be much slower than electron injection and electron transfer from I^- ion into oxidized dyes (i.e. regeneration of dyes) to accomplish effective charge separation. It was reported that charge recombination between injected electrons on TiO_2 and cations of N3 dye occurs on the order of microseconds to milliseconds, in contrast with ultrafast electron injection [28, 39, 40, 48–50]. The much slower charge recombination compared to electron injection leads to effective charge separation and consequently high cell performance. Charge recombination in the N3 dye/TiO_2 system is derived from electron transfer from TiO_2 to Ru(III), while electron injection occurs because of electron transfer from the bipyridyl ligand to TiO_2. Thus, it is considered that long-distance electron transfer from TiO_2 to the Ru metal center leads to a much smaller electron-transfer rate.

15.1.4.3 Regeneration of the oxidized photosensitizers

Electron transfer from the I^- ion into oxidized photosensitizers (cations), or regeneration of photosensitizers (Figure 15.9), is one of the primary processes needed to achieve effective charge separation. The kinetics of this reaction has also been investigated by time-resolved laser spectroscopy [48, 51]. The electron-transfer rate from the I^- ion into cations of the N3 dye was estimated to be 100 ns [48]. This reaction rate is much faster than that for charge recombination between injected electrons and dye cations. Thus, fast regeneration of the oxidized photosensitizer also contributes to the accomplishment of effective charge separation.

15.1.4.4 Recombination between injected electrons and tri-iodide ions (dark current)

Recombination of injected electrons with tri-iodide ions (I_3^-) on a semiconductor as shown in Figure 15.9, corresponding to dark current, is one of the primary processes in a DSSC (reaction [5]).

$$I_3^- + 2e^-(TiO_2) \rightarrow 3I^- \qquad [5]$$

This reaction can also occur on the SnO_2 surface because the nanocrystalline TiO_2 does not completely cover the TCO substrate, but predominantly occurs on the TiO_2 surface because of the high surface area of the TiO_2 relative to the SnO_2. This reaction contributes to the loss of PV performance in a DSSC analogous to the forward-bias injection of holes and electrons in a *p-n* junction. The V_{OC} in DSSC is obtained using the injection current, I_{inj}, as represented by the following equation, as well as *p-n* junction solar cells:

$$V_{OC} = \frac{kT}{q} \ln\left(\frac{I_{inj}}{I_0} + 1\right) \qquad (15.6)$$

where k is the Boltzmann constant, q is the magnitude of the electron charge, T is the absolute temperature, and I_0 is the dark current. I_{inj} and I_0 are represented by the following equations:

$$I_{inj} = q\eta\Phi_0 \qquad (15.7)$$

$$I_0 = q\, n_0 k_{et}[I_3^-] \qquad (15.8)$$

where η is the quantum yield for photogenerated electrons, Φ_0 is the incident photon flux, n_0 is the electron density on the conduction band of the semiconductor in the dark, k_{et} is the rate constant for recombination, reaction [5], and $[I_3^-]$ is the concentration of oxidized redox mediator, I_3^-, in the solution. From equations (15.6) to (15.8), we obtain the following equation:

$$V_{OC} = \frac{kT}{q} \ln\left(\frac{\eta\Phi_0}{n_0 k_{et}[I_3^-]} + 1\right) \qquad (15.9)$$

Usually, $\eta\Phi_0 \gg n_0 k_{et}[I_3^-]$ and equation (15.9) is simplified as follows [6, 12, 52, 53]:

$$V_{OC} = \frac{kT}{q} \ln\left(\frac{\eta\Phi_0}{n_0 k_{et}[I_3^-]}\right) \qquad (15.10)$$

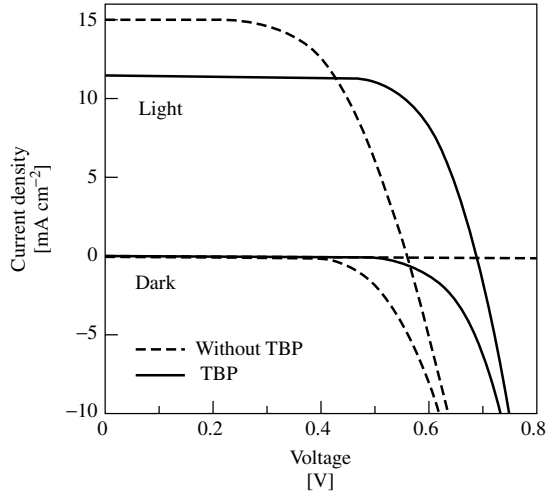

Figure 15.10 Current–voltage characteristics of N3 dye-sensitized TiO_2 solar cells under illumination and darkness using electrolyte with and without TBP: (— —) without TBP, (——) with TBP

Dark current is considered to occur at the TiO_2/electrolyte interface where the photosensitizers are not adsorbed. To suppress dark current, pyridine derivatives such as *tert*-butylpyridine (TBP) have been employed as coadsorbates on the TiO_2 surface, resulting in the improvement of photovoltage [6, 52]. TBP is considered to adsorb on the uncovered TiO_2 surface. Figure 15.10 shows the current–voltage characteristics of the N3 dye-sensitized TiO_2 solar cell under illumination and darkness, using electrolyte with and without TBP. This clearly indicates that TBP suppresses dark current, resulting in the improvement of V_{OC}. A decrease of the J_{SC} by addition of TBP is considered to be due to the negative shift of the conduction-band level of TiO_2 owing to adsorption of TBP, which has basic property, leading to suppression of the electron injection from the dye.

The kinetics of recombination, reaction [5], has been investigated and discussed [6, 52, 54–59]. If this reaction occurs predominantly with a large reaction rate, the DSSC does not work. Taking into consideration this and the slow transport of the photoinjected electrons through the nanocrystalline TiO_2 film (described in the next section), the recombination must be extremely slow. In fact, the rate of recombination has been estimated to be on the order of 0.1 s to several seconds [56]. This slow recombination would be due to a low electrocatalytic activity of TiO_2 for the reduction of tri-iodide ions.

15.1.4.5 Electron transport in TiO_2 film

Electron transport in TiO_2 film is an important process related to PV performance in the DSSC (see Figure 15.9) and has been studied by many researchers [60–74]. The electron transport in nanocrystalline TiO_2 film has been discussed with respect to different mechanisms: a diffusion model [60–63], a mechanism that involves tunneling through potential barriers between the particles [63], a trapping/detrapping mechanism [65–68], and an insulator–metal (Mott) transition mechanism [69]. Electron conductivity in TiO_2 is very small, resulting in slow response of the photocurrent. For example, diffusion

coefficients of the electrons in nanocrystalline TiO_2 film have been estimated to be 1×10^{-7} [60] and 1.5×10^{-5} $cm^2\,s^{-1}$ [61]. In the DSSC, the electron conductivity of TiO_2 film is significantly increased due to electron injection from photosensitizers under photon irradiation [62, 63]. In addition, conductivity and response of the photocurrent increase with increasing incident light intensity [62, 63]. It has been suggested that when injected electrons fill the trap site and/or surface levels in the TiO_2 film, the diffusion coefficient of the electron increases drastically, leading to elevated electron conductivity and good response of the photocurrent.

15.1.5 Characteristics

As described above, the photovoltaic (PV) mechanism of DSSC is different from that of conventional *p-n*-type solar cells. The DSSC has other unique characteristics such as the following:

1. *High energy conversion efficiency*: A DSSC efficiency equal to that of the amorphous-Si solar cell has been obtained during laboratory development and efficiencies greater than 10% may be possible.
2. *Low-cost fabrication*: The DSSC is very simple to construct and is made of low-cost materials. Fabrication costs will therefore be less than that for conventional solar cells. For example, US$0.60/W, which may be competitive for conventional solar cells, has been estimated for a DSSC with 10% efficiency [10, 15].
3. *Abundant supply of component materials*: Oxide semiconductors such as TiO_2, dye, and iodine are abundantly available. Although metal deposits of Ru are limited, the amount of Ru complex used in the DSSC is only 1×10^{-7} $mol\,cm^{-2}$. As discussed in Section 15.3.2.2, organic dye photosensitizers could be used rather than Ru complexes if resource limitation is a problem.
4. *Good potential for colorful, adaptable consumer products*: Colorful and transparent solar cells can be made using various kinds of dyes, depending on the use of the cell. For example, transparent solar cells could be used in place of windowpanes. Additionally, the use of a plastic substrate, rather than glass, is possible if low temperature processing of the TiO_2 film preparation ($<250^{\circ}C$) is available and would expand the use of DSSC.
5. *Low potential for environmental pollution*: The TiO_2, dyes, and iodine used in the DSSC are nontoxic. The only component that could potentially cause harm is the organic solvents used in the electrolyte solution. Future research should be directed toward developing a solid-state electrolyte.
6. *Good recyclability*: The organic dye photosensitizers adsorbed on the electrode can be removed by washing the electrode with alkali solutions or combustion, providing recyclability of the DSSC.

15.2 DSSC FABRICATION ($\eta = 8\%$)

15.2.1 Preparation of TiO_2 Colloid

Commercial powders of TiO_2, such as P25 (Degussa or Nippon Aerosil [75]), can be used to fabricate the TiO_2 photoelectrode. Colloidal TiO_2 prepared by hydrolysis of Ti(IV)

alkoxides, such as isopropoxide and butoxide, has usually been used to produce high-performance solar cells [16, 76]. Generally, the anatase phase rather than rutile phase of TiO_2 is more suitable for electrodes [77]. Preparation involves the following steps:

1. Precipitation by hydrolysis of Ti alkoxides using 0.1 M HNO_3.
2. Peptization by heating at 80°C for 8 h, followed by filtering.
3. Hydrothermal growth by autoclaving at 200 to 250°C for 12 h.
4. Sonication with an ultrasonic bath.
5. Concentration with an evaporator.

Precipitation involves controlled hydrolysis of a Ti alkoxide, such as Ti isopropoxide. To obtain monodispersed particles of the desired size, the hydrolysis and condensation kinetics must be controlled. Ti-alkoxides suitably modified with acetic acid or acetyl acetonate yield colloids having a large surface area ($>200\ m^2\ g^{-1}$) and smaller particle diameter (5–7 nm) [16, 76]. Peptization results in the segregation of the agglomerates to primary particles, after which the large agglomerates are removed by filtration. Autoclaving of the colloidal TiO_2 solution leads to growth of the primary particles to 10–25 nm and also to some extent increases the anatase crystallinity present. At higher autoclaving temperature, more growth of particles and rutile formation occur, particularly at temperatures above 240°C. Electrodes prepared using colloids autoclaved at or below 230°C are transparent, while those made from colloids autoclaved at higher temperatures are translucent or opaque. After autoclaving, the precipitates are redispersed using an ultrasonic processor equipped with a Ti-horn (e.g. Sonics & Materials Inc., 400–600 W [78]). The colloidal solution is then concentrated at 45°C using a rotary evaporator to reach desired concentration of approximately 11 wt% TiO_2.

15.2.2 Preparation of the TiO_2 Electrode

The TiO_2 thin film is usually prepared by one of the two methods:

(a) Doctor blade technique

To increase the porosity of the film, 0.02 to 0.07 g of polyethylene glycol (PEG, molecular weight 20 000) is added as a binder to 1 mL of the concentrated colloidal TiO_2 solution (TiO_2, 11 wt%). If a commercial powder such as P25 is used, the powder is dispersed by grinding with water, a particle stabilizer such as acetylacetone, and a nonionic surfactant such as Triton X [6]. The colloidal TiO_2 solution is spread on a TCO substrate and then sintered at 450°C for 30 min under air. The resulting TiO_2 film is transparent.

(b) Screen printing

The TiO_2 colloid is separated from acidified water, washed carefully, and then mixed with EC as a binder and α-terpineol as a solvent in ethanol, yielding an organic TiO_2 paste after evaporating ethanol. The paste is printed on a TCO substrate using a screen printing machine and then sintered at 500°C for 1 h under air. The film thickness is easily controlled in screen printing by the selection of paste composition (i.e. wt% of TiO_2 nanoparticles in the paste), screen mesh size, and repetition of printing.

Films prepared by both methods have film thicknesses of 5 to 15 μm and film mass of about 1 to 2 mg cm^{-2}. The optimum film thickness is 13 to 14 μm. The films have porosity of 60 to 70% [76]. High porosity produces effective diffusion of the redox mediator into the film. The roughness factor (shown above) for a 10-μm film reaches approximately 1000, allowing the adsorption of large amounts of photosensitizer and consequently increased light-harvesting efficiency, as described in Section 15.1.2.2. TiO_2 film prepared from 10 to 20 nm particles of TiO_2 is transparent.

The scattering property of the film is important for the improvement of the LHE of the dye-coated film, resulting in improved IPCE performance of the cell. This effect of the scattering in the TiO_2 film has been investigated in detail [16, 76, 79–82]. The path length of the incident light and therefore the absorption due to the adsorbed dye can be increased by light scattering in the TiO_2 film. This can be achieved by the addition of some larger TiO_2 particles in small TiO_2 particles during film preparation, since larger particles have small surface area and consequently cannot adsorb large amount of the dye. A simulation of light scattering in the TiO_2 electrode of DSSC predicts that a suitable mixture of small TiO_2 particles (e.g. 20 nm diameter) and of larger particles (250–300 nm diameter), which are effective light-scattering centers, have the potential to enhance solar light absorption significantly [80]. Actually, the photocurrent of DSSC increased by using a scattering film compared to that for a transparent film [81]. This improvement in the photoresponse of DSSC due to the scattering effect is observed especially in the low-energy region (e.g. 650–900 nm). As shown in Figures 15.4 and 15.7, the IPCE values obtained in the red region are higher than what is indicated by the absorption spectra of the dyes in solution (Figure 15.4, $1 - T$). On the low-energy side, a significant part of the incident radiation penetrates the layer due to the low absorption coefficient of the dye, while photons of 500 to 650 nm can be mainly absorbed near the TCO/TiO_2 interface because of the large absorption coefficient. Multiple reflections of the low-energy light in highly scattering films result in increased light absorption and hence increased photoresponse than what the solution absorption spectra indicate.

It has also been reported that $TiCl_4$ treatment of the film significantly improves cell performance, especially the photocurrent [6]. After printing, the TiO_2 films are immersed in 0.1 to 0.5 M $TiCl_4$ aqueous solutions at room temperature and then sintered at 450°C for 30 min. It is possible that $TiCl_4$ treatment improves the photocurrent by improving the connections between TiO_2 particles.

15.2.3 Dye Fixation onto the TiO_2 Film

After preparation of the TiO_2 films, the N3 dye photosensitizer is adsorbed onto the TiO_2 surface. The films are immersed into the dye solution (0.2–0.3 mM in ethanol or *tert*-butanol–acetonitrile, 1:1 mixed solution) followed by storage at room temperature for 12 to 18 h. This treatment produces intense coloration of the film. Before use, the film is washed with alcohol or acetonitrile to remove excess nonadsorbed dyes inside the nanoporous TiO_2 film.

15.2.4 Redox Electrolyte

As described in Section 15.1.2.4, organic solutions containing iodine redox ions have been used as the redox electrolyte. Typical organic solvents are nitrile solvents having relative low viscosity, such as acetonitrile, propionitrile, methoxyacetonitrile, and methoxypropionitrile, which produce a high degree of ion conductivity. It has been reported that imidazolium derivatives, such as 1,2-dimethyl-3-hexylimidazolium iodide (DMHImI) and 1,2-dimethyl-3-propylimidazolium iodide (DMPImI), decrease the resistance of the electrolyte solution and improve photovoltaic performance [83, 84]. A typical electrolyte composition that produces high solar cell performance for the Ru complex photosensitizers reported by Grätzel's group is a mixture of 0.5 M DMHImI, 0.04 M LiI, 0.02 M I_2, and 0.5 M *tert*-butylpyridine (TBP) in acetonitrile [76]. As discussed earlier, TBP shifts the conduction-band level of the TiO_2 electrode to the negative direction and suppresses the dark current that corresponds to the reduction of I_3^- ions by injected electrons, leading to the improvement of the voltage [6, 52].

15.2.5 Counter Electrode

Sputtered Pt on a TCO substrate (5–10 $\mu g\,cm^{-2}$, or 200-nm thickness) has been usually employed as a counter electrode. When Pt is sputtered producing a mirrorlike effect, the photocurrent is slightly increased due to the light-reflection effect. In addition, the electrocatalytic activity of the Pt-sputtered TCO electrode for the reduction of tri-iodide ions is improved by the formation of Pt colloids on the surface [85]. Small amounts of an alcoholic solution of H_2PtCl_6 are dropped on the surface of the Pt-sputtered TCO substrate, followed by drying and heating at 385°C for 10 min, resulting in the formation of Pt colloids on the surface. The properties of the Pt counter electrode directly affect the fill factor of the solar cell. A desirable exchange current density corresponding to the electrocatalytic activity for the reduction of tri-iodide ions is 0.01 to 0.2 $A\,cm^{-2}$ [16, 85].

15.2.6 Assembling the Cell and Cell Performance

We can easily fabricate an unsealed DSSC and measure its PV performance. A spacer film, such as polyethylene (15- to 30-μm thickness), is placed on the dye-coated TiO_2 photoelectrode and then the electrolyte solution is dropped on the surface of the TiO_2 electrode using a pipette (one or two drops). The counter electrode is placed on top of the TiO_2 electrode, and then the two electrodes are fastened together with two binder clips. If a low melting point polymer film such as Surlyn is used instead of the spacer film, we can fabricate a sealed cell after packaging of the cell using a resin (e.g. ethylene vinyl acetate, EVA) for long-term stability.

Since Grätzel and coworkers reported high performance of a DSSC in 1991, many workers worldwide have tried to reproduce their result. Some reported performances are shown in Table 15.1. These cells were fabricated using a Ru complex photosensitizer, N3 dye, and a nanocrystalline TiO_2 electrode. In many cases, the light condition is AM1.5

Table 15.1 Photovoltaic performance of N3 dye-sensitized TiO_2 solar cells

Institute	Cell size [cm^2]	J_{SC} [$mA\,cm^{-2}$]	V_{OC} [mV]	Fill factor	η [%]	Light source	Year
EPFL	0.31	18.2	720	0.73	9.6	AM1.5	1993
EPFL-NREL	0.17	18.6	740	0.73	10.0	AM1.5	1997
Uppsala Univ.	1.0	30.4	610	0.37	6.9	ELH lamp	1994
ISK	0.5	14.2	630	0.71	6.3	AM1.5	1994
Osaka Univ.	0.5	3.9	570	0.67	6.1	21 mW cm^{-2}	1995
NREL	0.44	14.5	730	0.71	7.5	AM1.5	1997
NIMC	0.13	14.5	698	0.71	7.2	AM1.5	1998
EPFL-NIMC	0.21	15.2	780	0.71	8.4	AM1.5	1999
INAP	144	–	–	–	7.0	AM1.5	1997

EPFL: Swiss Federal Institute of Technology, Switzerland
NREL: National Renewable Energy Laboratory, USA
ISK: Ishihara Sangyo Kaisha Ltd
NIMC: National Institute of Materials and Chemical Research, Japan
INAP: Institut für Angewandte Photovoltaik GmbH, Germany

(approximately 100 mW cm^{-2}) produced with a solar simulator in the laboratory. Grätzel and coworkers reported $\eta = 9.6\%$ in 1993, and they achieved 10% at NREL in 1997. Other high efficiencies were reported by Lindquist and coworkers, at Uppsala University (6.9%, 1994), NREL (7.5%, 1997), Ishihara Sangyo Kaisha Ltd. in Osaka (6.3%, 1994), and Yanagida and coworkers at Osaka University (6.1%, using 21 mW cm^{-2}, 1995). Our group achieved 7.2% in 1998, 8.4% in cooperation with EPFL in 1999, and 8.3% in cooperation with Sumitomo Osaka Cement Co. Ltd. in 2000. A venture company, Institut für Angewandte Photovoltaik GmbH (INAP), that has been investigating commercialization of the DSSC in cooperation with EPFL achieved 7% in 1997 using a 144 cm^2 cell (12×12 cm^2). Although these groups have reproduced efficiency values greater than 7%, additional studies must be done to reproduce 10% efficiency.

The establishment of standard measurement conditions for cell performance of DSSC is necessary before cell performance can be estimated exactly because performance depends on measurement conditions, such as light intensity and spectrum. Generally, under low light intensity, fill factor of DSSC is improved because of low photocurrent (i.e. low series resistance), resulting in improved cell performance. The light whose intensity and spectrum are close to AM1.5 irradiation should be used as the light source similar to conventional solar cells. Spectral response (IPCE) performance of DSSCs also depends on light conditions [63]. DSSCs show relatively slow response because of low electron mobility of the TiO_2 film, as described in Section 15.1.4.5. Under high-intensity irradiation, the response of DSSCs increase with electron injection and electron trap filling. Therefore, IPCE performance should be measured by a DC method with high-intensity monochromatic light or an AC method using white bias irradiation and low chopper frequencies (e.g. <50 Hz [63]).

15.3 NEW DEVELOPMENTS

DSSCs producing current with 10% efficiency using a Ru complex photosensitizer and a nanocrystalline TiO_2 photoelectrode have been shown to be a significant new type

of highly efficient solar cell in addition to the conventional *p-n* type solar cells. Basic and theoretical studies of DSSCs and attempts to commercialize them have been intensively pursued. This section discusses recent approaches to improve cell performance and commercialize DSSCs.

15.3.1 New Oxide Semiconductor Film Photoelectrodes

To date, nanocrystalline TiO_2 electrodes have been used predominantly as the photoelectrode in DSSCs, but other oxide semiconductor materials, ZnO [23, 86–92], SnO_2 [23, 51, 91–93], Nb_2O_5 [23, 43, 91, 92], In_2O_3 [23, 91, 92], $SrTiO_3$ [94], and NiO [95], have also been investigated (Table 15.2). Nevertheless, nanocrystalline TiO_2 electrodes have the best performance, and oxide semiconductor materials exceeding the performance of TiO_2 have not been found. The physical properties of the materials, such as the energy level of the conduction band and the electron conductivity, influence the performance of the photoelectrode significantly, affecting cell performance.

Recently, combined photoelectrodes consisting of two oxide semiconductor materials have also been investigated [96–98]. Tennakone and coworkers reported that a DSSC based on a nanocrystalline SnO_2/ZnO-combined photoelectrode and N3 dye produced a highly efficient cell performance equal to that of the TiO_2 solar cell [96, 97]: 8% η($J_{SC} = 22.8$ mA cm^{-2}, $V_{OC} = 0.67$ V, and $ff = 0.50$) under 90 mW cm^{-2} and 15% η under 10 mW cm^{-2} [96]. They employed a combined film consisting of small particles of SnO_2 (15 nm) and large particles of ZnO (2 μm, 53 wt%). The performance of the combined photoelectrode was improved drastically compared to that of ZnO and SnO_2 electrodes. It is believed that the Ru complex is adsorbed on SnO_2 nanoparticles, and ZnO contributes to the electron-transfer process. These results indicate the possibility of developing non-TiO_2, high-performing electrodes for DSSC, although the detailed mechanism of the new electrode has not been elucidated at this time.

The effect on performance of coating the surface of the TiO_2 electrode with other oxide compounds has been investigated by several groups. Zaban *et al*. prepared a nanocrystalline TiO_2 electrode coated with Nb_2O_5, whose conduction-band level is more negative than that of TiO_2. They measured cell performance of a DSSC using this photoelectrode and N3 dye [99]; the J_{SC} and V_{OC} were improved compared to those of the TiO_2 electrode. Wang *et al*. studied cell performance of DSSC using a nanocrystalline ZnO-modified TiO_2 photoelectrode and N3 dye [100]. In this study, the J_{SC} and V_{OC} were also improved compared to those of the TiO_2 electrode. They believed that the improvement was caused by a positive shift of the conduction-band level of the photoelectrode and suppression of dark current due to the ZnO coating [100].

15.3.2 New Dye Photosensitizers

15.3.2.1 Metal complex photosensitizers

As described in Section 15.1.2.3, the $RuL_2(NCS)_2$ complex (N3 dye), and $RuL'(NCS)_3$ complex (Black dye), were developed and investigated intensively as photosensitizers. Other Ru complex photosensitizers have also been synthesized and characterized, and their

Table 15.2 Photovoltaic performance of dye-sensitized oxide semiconductor solar cells

Reference	Electrode	Dye	Conditions	Performance
[83]	ZnO	N3	56 mW cm^{-2}	$\eta = 2\%$
[87]	ZnO	Mercurochrome	AM1.5 (99 mW cm^{-2}), 0.09 cm^2	$\eta = 2.5\%$ ($J_{SC} = 7.4$ mA cm^{-2}, $V_{OC} = 0.52$ V, $ff = 0.64$)
[87]	SnO_2	Mercurochrome	AM1.5 (100 mW cm^{-2}), 0.25 cm^2	$\eta = 0.65\%$ ($J_{SC} = 2.0$ mA cm^{-2}, $V_{OC} = 0.58$ V, $ff = 0.56$)
[87]	In_2O_3	Mercurochrome	AM1.5 (100 mW cm^{-2}), 0.25 cm^2	$\eta = 0.38\%$ ($J_{SC} = 5.4$ mA cm^{-2}, $V_{OC} = 0.24$ V, $ff = 0.29$)
[23]	Nb_2O_5	N3	520 nm (4 mW cm^{-2}), 1 cm^2	$\eta = 2.6\%$ ($J_{SC} = 0.29$ mA cm^{-2}, $V_{OC} = 0.61$ V, $ff = 0.58$)
[88]	Nb_2O_5	N3	Xe lamp (100 mW cm^{-2}), UV and IR cut off	$\eta = 1.2\%$ ($J_{SC} = 3.3$ mA cm^{-2}, $V_{OC} = 0.67$ V, $ff = 0.54$)
[90]	$SrTiO_3$	N3	AM1.5 (1 sun)	$\eta = 1.8\%$ ($J_{SC} = 3$ mA cm^{-2}, $V_{OC} = 0.789$ V, $ff = 0.70$)
[92]	SnO_2/ZnO	N3	90 mW cm^{-2}	$\eta = 8\%$ ($J_{SC} = 22.8$ mA cm^{-2}, $V_{OC} = 0.67$ V, $ff = 0.5$)
[94]	Nb_2O_5/TiO_2	N3	Xe lamp	$J_{SC} = 11.4$ mA cm^{-2}, $V_{OC} = 0.732$ V, $ff = 0.564$
[95]	TiO_2/ZnO	N3	Xe lamp (81 mW cm^{-2}), UV and IR cutoff	$\eta = 9.8\%$ ($J_{SC} = 21.3$ mA cm^{-2}, $V_{OC} = 0.71$ V, $ff = 0.52$)
[88]	Nb_2O_5/TiO_2	N3	Xe lamp (100 mW cm^{-2}), UV and IR cutoff	$\eta = 2.0\%$ ($J_{SC} = 7.1$ mA cm^{-2}, $V_{OC} = 0.68$ V, $ff = 0.42$)
[91]	NiO (p-type)	erthrosin B	68 mW cm^{-2}	$J_{SC} = 0.2$ mA cm^{-2}, $V_{OC} = 0.08$ V
[98]	Y_2O_3/SnO_2	N3	AM1.5 (100 mW cm^{-2})	$\eta = 4.9\%$ ($J_{SC} = 13.8$ mA cm^{-2}, $V_{OC} = 0.61$ V, and $ff = 0.59$)

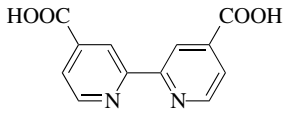

4, 4'-Dicarboxy-2, 2'-bipyridine [6, 103]

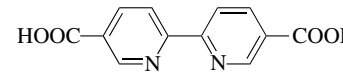

5, 5'-Dicarboxy-2, 2'-bipyridine [102]

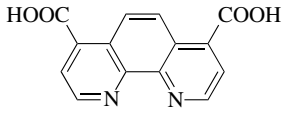

4, 7-Dicarboxy-1, 10-phenanthroline [111, 115, 117]

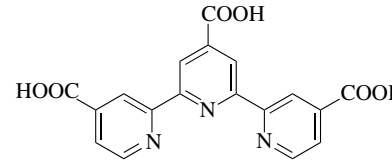

4, 4', 4"-Tricarboxy-2, 2':6', 2"-terpyridine [7, 8, 122]

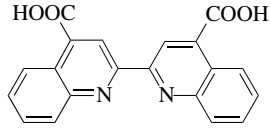

4, 4'-Dicarboxy-2, 2'-biquinoline [103, 114]

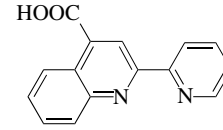

4-Carboxy-2-(2'-pyridyl)quinoline [121]

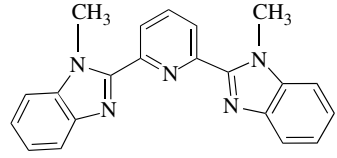

2, 6-Bis(1-methylbenzimidazol-2-yl) pyridine [103]

Figure 15.11 Molecular structures of ligands for Ru complex photosensitizers

performances as photosensitizers in the DSSC have been reported by many researchers [101–122]. Several ligands for Ru complex photosensitizers are shown in Figure 15.11 and the structures of new metal complex photosensitizers and their absorption properties are shown in Figure 15.12. The *y*-axis is represented by molar absorption coefficient, ε (i.e. absorption coefficient per M, unit M^{-1} cm^{-1}).

For example, a Ru phenanthroline complex, *cis*-bis(4,7-dicarboxy-1,10-phenanthroline)dithiocyanato ruthenium(II) ($Ru(dcphen)_2(NCS)_2$), which has absorption properties due to MLCT transition with a maximum near 520 nm, similar to N3 dye, has been synthesized and characterized [111, 115, 117], and an efficiency value of 6.1 to 6.6% under AM1.5 was obtained using a nanocrystalline TiO_2 solar cell. It has been reported that a Ru bipyridyl complex having an acetylacetonato ligand instead of two thioisocyanato ligands (-NCS) also showed high performance as a photosensitizer [118]. A Ru biquinoline complex, whose absorption due to MLCT transition is red-shifted compared to that of N3 dye, has also been synthesized [114]. Because the LUMO level of this complex is not sufficiently negative to inject electrons effectively, high solar cell performance has not been obtained with a nanocrystalline TiO_2 electrode, although electron injection from this complex into a nanocrystalline SnO_2 electrode, whose conduction-band level is more positive than that of TiO_2, occurs effectively [114]. Tuning of both the LUMO and the HOMO levels of the complex to inject electrons effectively into the conduction band

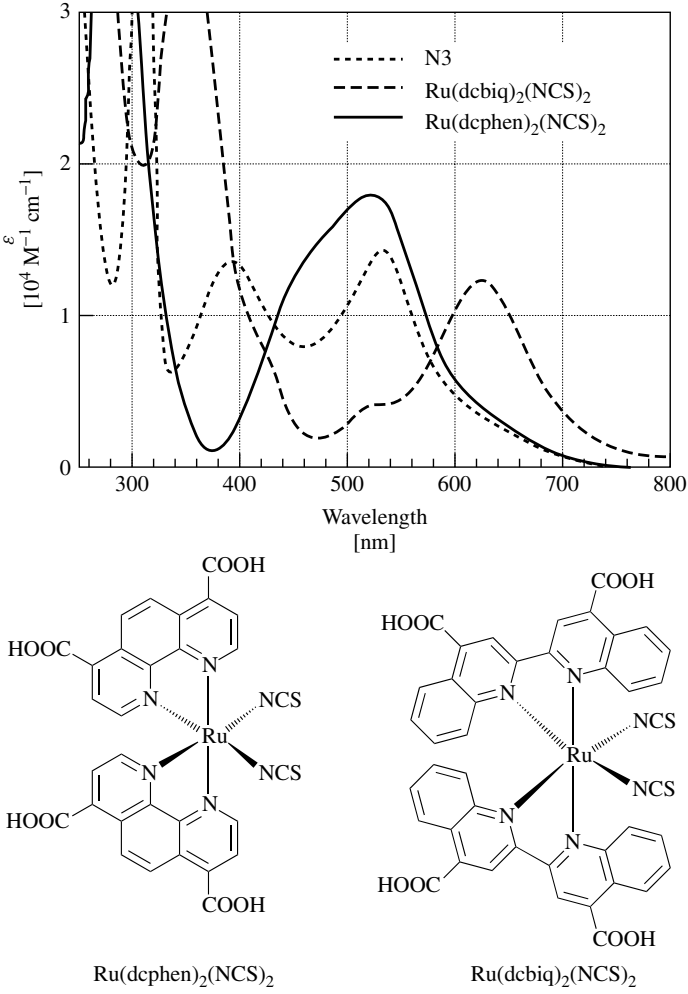

Figure 15.12 Molecular structures of new metal complex photosensitizers, $Ru(dcphen)_2(NCS)_2$ and $Ru(dcbiq)_2(NCS)_2$, and their absorption properties in ethanolic solution: (– – –) N3 dye [6, 103], (— —) $Ru(dcbiq)_2(NCS)_2$ [103, 114], (——) $Ru(dcphen)_2(NCS)_2$ [111, 115, 117]. The *y*-axis is represented by molar absorption coefficient, ε

of the semiconductor electrodes and accept electrons from I^- ions, respectively, is very important in developing new efficient photosensitizers.

Metal complexes having metal centers other than Ru have also been synthesized and their performance have been investigated. These include Fe complexes [123, 124], Os complexes [125–128], Re complexes [129], and Pt complexes [130]. A nanocrystalline TiO_2 solar cell sensitized by a square-planar platinum (II) complex containing 4,4′-dicarboxy-2,2′-bipyridine and quinoxaline-2,3-dithiolate ligands showed an efficiency of 2.6% ($J_{SC} = 6.14$ mA cm^{-2} and $V_{OC} = 0.60$ V) under simulated AM1.5 solar irradiation [130]. However, highly efficient performance exceeding that of the Ru complex

photosensitizers has not been attained. This is believed to be because the HOMO level of Ru complexes derived from the d orbitals of the Ru metal center (i.e. the redox potential of Ru(II)/Ru(III)) is best matched to the iodine redox potential to accept electrons effectively.

Porphyrin [131–134] and phthalocyanine [135] derivatives have also been employed as photosensitizers in the DSSC. A nanocrystalline TiO_2 solar cell sensitized by Cu chlorophyllin produced 2.6% efficiency ($J_{SC} = 9.4$ mA cm^{-2} and $V_{OC} = 0.52$ V) under 100 mW cm^{-2} [131]. To develop new efficient metal complex photosensitizers, an increase in the absorption coefficient of the metal complex as well as an increase in the red shift of the absorption region is needed because the absorption coefficient decreases as the red shift increases.

15.3.2.2 Organic and natural dye photosensitizers

Organic dyes whose HOMO and LUMO levels match the conduction-band level of the semiconductor and the iodine redox potential can also be utilized as photosensitizers. As described in Section 15.1.1, organic dyes such as 9-phenylxanthene dyes were used as photosensitizers in early researches. Organic dyes have several advantages as photosensitizers: (1) they have a variety of structures for molecular design, (2) they are cheaper than metal complexes, and (3) they have large absorption coefficients attributed to intermolecular $\pi-\pi^*$ transition. Construction of nanocrystalline DSSCs using organic dye photosensitizers has been reported, and some structures are shown in Figure 15.13 [90, 91, 136–145].

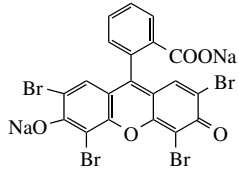

Eosin yellow [137]

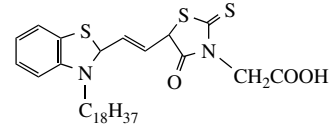

Merocyanine dye [141]

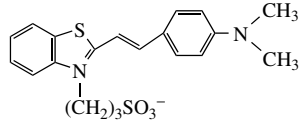

Cyanine dye [139, 140]

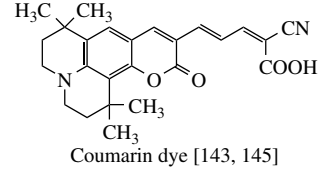

Coumarin dye [143, 145]

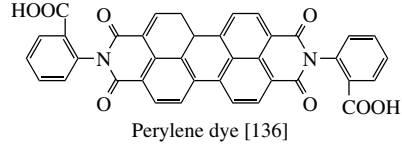

Perylene dye [136]

Figure 15.13 Molecular structures of organic dye photosensitizers

A nanocrystalline SnO_2 solar cell sensitized by a perylene derivative produced 0.9% efficiency under AM1.5 ($J_{SC} = 3.26$ mA cm^{-2} and $V_{OC} = 0.45$ V) [136]. With a TiO_2 solar cell (1 cm^2) sensitized by eosin yellow, one of the 9-phenylxanthene dyes produced 1.3% efficiency ($J_{SC} = 2.9$ mA cm^{-2}, $V_{OC} = 0.66$ V, and $ff = 0.67$) [137]. A mercurochrome/ZnO solar cell (0.09 cm^2) attained 2.5% efficiency ($J_{SC} = 7.44$ mA cm^{-2}, $V_{OC} = 0.52$ V, and $ff = 0.64$) under AM1.5 irradiation [90, 91].

Cyanine and merocyanine dyes have also been used as photosensitizers [138–142]. A nanocrystalline TiO_2 solar cell based on a merocyanine dye photosensitizer (surface area, 0.25 cm^2) produced an efficiency of 4.2% ($J_{SC} = 9.7$ mA cm^{-2}, $V_{OC} = 0.62$ V, and $ff = 0.69$) under AM1.5 (100 mW cm^{-2}) [141]. Aggregates of the merocyanine dye formed on the TiO_2 surface result in expansion of the absorption area, especially in the long-wavelength region, resulting in improvement of light-harvesting performance [141].

We synthesized new coumarin derivatives that can absorb visible light from 400 to 700 nm and prepared nanocrystalline TiO_2 solar cell. Under AM1.5 irradiation, an efficiency of 5.6% was attained (area = 0.25 cm^2, $J_{SC} = 13.8$ mA cm^{-2}, $V_{OC} = 0.63$ V, and $ff = 0.64$) [143, 145] (recently we attained 6.0% efficiency). A maximum IPCE of 76% was obtained at 470 nm. The photocurrent performance of this solar cell is almost equal to that of the N3 dye/TiO_2 solar cell, indicating a promising prospect for organic dye photosensitizers. Design and development of new organic dyes with absorption in the near-IR region and large absorption coefficients are needed to improve DSSC performance using organic dye photosensitizers.

In addition to organic dyes, natural dyes extracted from plants can also be used as photosensitizers [34, 146, 147]. A nanocrystalline TiO_2 solar cell using a santalin dye extracted from red sandalwood can produce 1.8% efficiency under 80 mW cm^{-2} irradiation [147]. Cherepy *et al*. reported that a nanocrystalline TiO_2 solar cell using flavonoid anthocyanin dyes extracted from blackberries can convert sunlight to electrical power at an efficiency of 0.6% ($J_{SC} = 1.5 - 2.2$ mA cm^{-2} and $V_{OC} = 0.4 - 0.5$ V) under AM1.5 [34]. The maximum IPCE was 19% at the peak of the visible absorption band of the dye. They also observed a fast electron injection of <100 fs from cyanin dye into the conduction band of TiO_2 as measured by time-resolved transient absorption spectroscopy [34].

15.3.3 New Electrolytes

Room-temperature ionic liquids (molten salts) have been extensively studied as replacements for volatile organic solvents in electrochemical devices such as batteries because of their high ionic conductivity, electrochemical stability, and nonvolatility. Of these properties, nonvolatility is the most critical for ensuring the long-term stability of electrochemical devices. Such room-temperature ionic liquids have also been utilized and studied in DSSCs in place of liquid electrolytes [84, 148]. Ionic liquids used in DSSCs include imidazolium derivatives, such as 1-hexyl-3-methylimidazolium iodide (HMImI) [84] and 1-ethyl-3-methylimidazolium bis(trifluoromethylsulfonyl)imide (EMIm-TFSI) [148]. Matsumoto *et al*. reported that an N3 dye-sensitized TiO_2 solar cell using an EMIm salt having hydrofluoride anions, $H_2F_3^-$ or $H_3F_4^-$, as the electrolyte solvent produced 2.1% efficiency under AM1.5 ($J_{SC} = 5.8$ mA cm^{-2}, $V_{OC} = 0.65$ V, and $ff = 0.56$) [148]. If the viscosity

of these ionic liquids can be decreased similarly to that of organic solvents, the solar cell performance will be improved as a result of increased ionic mobility of the electrolyte.

15.3.4 Quasi-solid-state and Solid-state DSSCs

Development of solid-state or quasi-solid-state DSSCs is essential for developing a cell with long-term stability and is critical for commercialization. Because liquid electrolytes using organic solvents are usually utilized in conventional DSSCs, techniques for sealing the cell must be perfectly established to prevent evaporation of components of the electrolyte especially under high temperatures in outdoor applications. In addition, the solid-state DSSC would allow easier interconnection of a cell into a monolithic module.

Grätzel and coworkers studied an N3 dye-sensitized nanocrystalline TiO_2 solar cell using a hole-transport material, 2,2′,7,7′-tetrakis(*N*,*N*-di-*p*-methoxyphenyl-amine)9,9′-spirobifluorene (OMeTAD), as a solid electrolyte (Figure 15.14) [149]. OMeTAD is

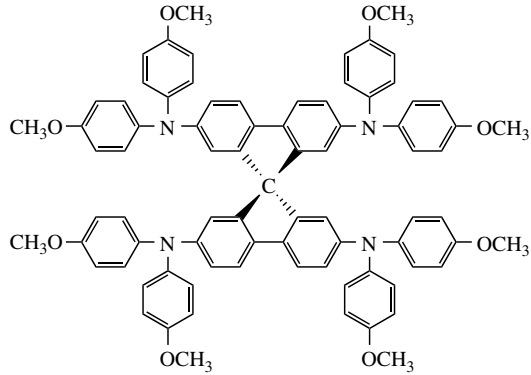

OMeTAD

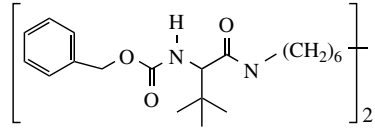

L-valine derivative galator

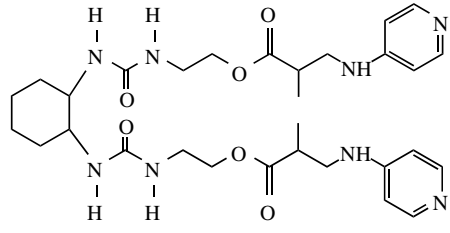

Gelator reported by Toshiba

Figure 15.14 Molecular structures of a solid-state electrolyte and gelator

spin-coated on the surface of the N3 dye/TiO_2 electrode and then Au is deposited by vacuum evaporation as the counter electrode, resulting in a sandwich-type DSSC. The cell efficiency was 0.7% under 9.4 mW cm^{-2} irradiation, and a J_{SC} of 3.18 mA cm^{-2} was obtained under AM1.5 (100 mW cm^{-2}) [149]. The maximum IPCE was 33%. The rate of electron injection from OMeTAD into cations of N3 dyes has been estimated as 3 ps, which is faster than that from I^- ions [150].

Tennakone and coworkers utilized a *p*-type semiconductor material, CuI (band gap, 3.1 eV), as a hole conductor and fabricated a solid-state DSSC [147, 151, 152]. Acetonitrile solution of CuI is dropped into the surface of the dye-coated TiO_2 film heated at approximately 60°C and then is diffused inside the film. After evaporation of the acetonitrile, CuI is deposited into nanoporous TiO_2 film. Au-coated TCO substrate as the counter electrode is pressed onto the surface of the TiO_2/dye/CuI film. In a system using santalin dye as the photosensitizer, 1.8% efficiency was obtained under 80 mW cm^{-2} irradiation [147] and the efficiency reached 4.5% for the TiO_2/N3 dye/CuI/Au system, suggesting the possibility that a highly efficient solid-state DSSC could be produced [151]. In these systems, CuI is considered to be partially in contact with TiO_2, decreasing cell performance owing to the recombination of injected electrons. To increase cell performance, there must be decreased TiO_2/CuI contact. Solid-state DSSCs have been studied using other organic and inorganic hole conductor materials, *p*-type CuSCN [153, 154], polypyrrole [155], and polyacrylonitrile [97].

Quasi-solidification of the electrolyte using a gelator is another method for replacing liquid electrolytes in a DSSC. Gelation can be accomplished by adding gelator into the electrolyte without other changes in the components of the electrolyte. Yanagida and coworkers studied gelation of the electrolyte using L-valine derivatives (Figure 15.14) as a gelator and measured solar cell performance of DSSCs using gel electrolytes [156]. The gelator was added at a concentration of 0.1 M and then dissolved at 90 to 140°C. The gel solution was poured onto the dye-coated TiO_2 film and then cooled. Interestingly, the performance of DSSCs using a gel electrolyte has been almost the same as that using a liquid electrolyte. Good long-term stability of the sealed cell using the gel electrolyte was obtained compared to that of a sealed cell using a liquid electrolyte.

Recently, Hayase and coworkers (Toshiba Co.) reported constructing a highly efficient DSSC using a gel electrolyte [157, 158]. The chemical structure of one of the gelator materials is shown in Figure 15.14. The gelator was dissolved in the electrolyte at high temperature, and consequently the gel solution was deposited on the dye-coated TiO_2 electrode surface and then cooled. One electrolyte composition they reported is a mixture of a gelator shown in Figure 15.14 (0.1 g), 1-methyl-3-propylimidazolium (10 g), I_2 (0.1 g), and 1,2,4,5-tetrakisbromomethylbenzene (0.1 g). Gelation is caused by polymerization between nitrogen and halogen compounds. A high efficiency, 7.3% (J_{SC} = 17.6 mA cm^{-2}, V_{OC} = 0.60 V, and ff = 0.68), was obtained for an N3 dye-sensitized TiO_2 solar cell using the gel electrolyte under AM1.5 irradiation, compared to 7.8% for a solar cell based on a liquid electrolyte. They concluded that the resistance of the electrolyte did not increase as a result of the gelation because no change of the fill factor was observed. The photocurrent increased linearly with increasing incident light intensity of up to 100 mW cm^{-2}, as well as a liquid DSSC. This suggests that gelation of the electrolyte does not suppress diffusion of I^- and I_3^- ions in the electrolyte.

15.4 APPROACH TO COMMERCIALIZATION

15.4.1 Stability of the DSSC

For commercialization of the DSSC to be successful, the cell and module must have long-term stability. In this section, studies of photochemical, chemical, and physical stability of the component materials of the DSSC and recent investigations concerning long-term stability of the cell will be discussed.

15.4.1.1 Photochemical and physical stability of materials

The photostability and thermal stability of Ru complexes have been investigated in detail [6, 159–162]. For example, it has been reported that the NCS ligand of the N3 dye, *cis*-Ru(II)(dcbpy)$_2$(NCS)$_2$ (dcbpy = 2,2′-bipyridyl-4,4′-dicarboxylic acid), is oxidized to a cyano group (–CN) under photo-irradiation in methanol solution, as measured by UV–Vis absorption spectroscopy and nuclear magnetic resonance (NMR) spectroscopy [6, 159]. In addition, the intensity of the IR absorption peak attributed to the NCS ligand starts to decrease at 135°C, and decarboxylation of N3 dyes occurs at temperatures above 180°C [161]. Desorption of the dye from the TiO_2 surface has been observed at temperatures above 200°C.

It has been considered that high stability of the dye can be obtained in a DSSC system by including I^- ions as the electron donor to dye cations. Degradation of the NCS ligand to a CN ligand due to an intramolecular electron-transfer reaction producing Ru(II) from Ru(III) occurs within 0.1 to 1 s [159], while the rate of reduction of Ru(III) to Ru(II) due to electron transfer from I^- ions into the dye cations is on the order of nanoseconds [28]. This indicates that one molecule of N3 dye can contribute to the photon-to-current conversion process with a turnover number of at least 10^7 to 10^8 without degradation [159]. Taking this into consideration, N3 dye is considered to be sufficiently stable in the redox electrolyte under irradiation.

We must also take into consideration the photoelectrochemical and chemical stability of the solvent in the electrolyte. Organic solvents employed in DSSCs are, for example, propylene carbonate, acetonitrile, propionitrile, methoxyacetonitrile, methoxypropionitrile, and their mixtures. It is known that carbonate solvents, such as propylene carbonate, decompose under illumination, resulting in the formation of a carbon dioxide bubble in the cell. Methoxyacetonitrile (CH_3O-CH_2CN) reacts with trace water in the electrolyte to produce the corresponding amide ($CH_3O-CH_2CONH_2$), which decreases the conductivity of the electrolyte [163]. Acetonitrile and propionitrile are considered to be relatively stable, giving 2000 h of stability under dark conditions at 60°C [163].

The stability of vapor-deposited Pt electrocatalyst on a TCO substrate used as a counter electrode has also been investigated. It was reported that the electrocatalytically active Pt layer did not seem to be chemically stable in an electrolyte consisting of LiI and I_2 dissolved in methoxypropionitrile [164].

15.4.1.2 Long-term stability of the cell

Professor Grätzel observed that a DSSC using an N3 dye and a nanocrystalline TiO_2 photoelectrode showed good long-term stability, which is due to effective photo-induced

electron transfer from the Ru complex photosensitizer into the conduction band of the semiconductor and from the iodine redox mediator to the photosensitizer. The number of electrons produced by one photosensitizer molecule (turnover number) reaches 500 million, corresponding to continuous stability for 10 years under irradiation.

Long-term stability of the DSSC is currently being investigated for commercial applications at EPFL, Solaronix S.A. in Geneva, the Netherlands Energy Research Foundation (ECN), INAP, and NIMC [6, 13, 159, 163, 165–167], shown in Table 15.3. For example, 7000 h of cell stability, which corresponds to 6 years of outdoor use, has been obtained under 1000 $W\,cm^{-2}$ with a UV cutoff filter, as shown in Figure 15.15 [159]. Späth and coworkers conducted DSSC stability tests at Solaronix with polymer-sealed devices containing viscous electrolytes with a high boiling point, such as glutaronitrile [165]. They discovered that no significant degradation of stability occurred over a period of 9600 h of continuous illumination at 35°C, indicating chemical stability of components and a physically stable seal using polymer materials. In addition, long-term stability of a small cell for more than 10 000 h has also been accomplished under no UV light conditions at 17°C at 2.5 suns using an electrolyte of 0.5 M LiI, 0.05 M I_2, and 0.3 M TBP in methoxypropionitrile [163]. Stability tests under UV irradiation have also been carried out [167]. Addition of MgI_2 to the electrolyte can significantly improve stability to UV light, resulting in stable PV performance for more than 1500 h under UV irradiation [167]. A detailed mechanism of the UV-stabilizing effect due to MgI_2 has not been elucidated.

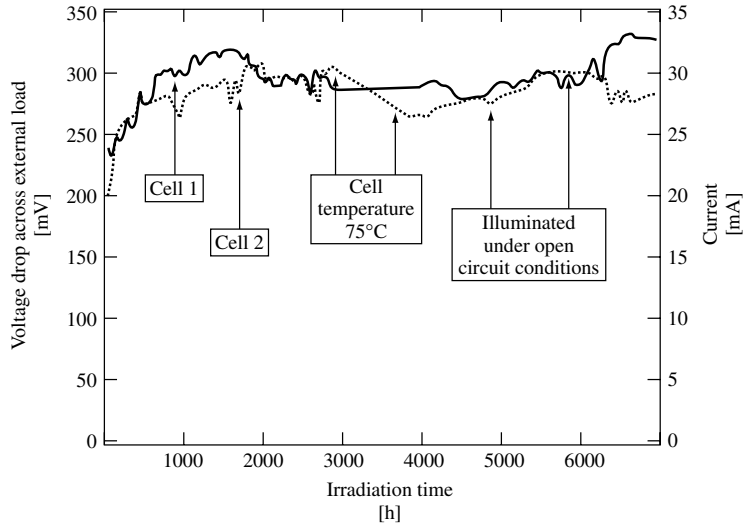

Figure 15.15 Stability test carried out with two sealed DSSCs over 7000 h of continuous illumination with visible light (polycarbonate 395-nm cutoff filter) at 1000 Wm^{-2} light intensity. The photocurrent and voltage drop measured across an external load resistor of 10 Ω are plotted as a function of irradiation time. Cell 1 (solid line) was continuously illuminated at 35°C; the same for cell 2 (broken line) except that it was operated for a 700-h period at 75°C and for 1000 h at open circuit. Reproduced from Kohle O, Grätzel M, Meyer A, Meyer T, *Adv. Mater.* **9**, 904–906 (1997) by permission of Wiley-VCH, STM-Copyright & Licenses [159]

Table 15.3 Long-term stability test of dye-sensitized TiO_2 solar cells

Institute and reference	Dye	Test conditions	Components	Term	Results
EPFL [6]	N3	150 W W-halogen lamp UV cutoff, 50°C	LiI/LiI_3 in PC or NMO	10 months	J_{SC}: 20–30% decreased initially. Passed charge: 10^5 C cm^{-2}, 10^7 turnovers.
EPFL [13]	N3	800 W m^{-2} Xe lamp UV cutoff	TBAI, I_2 in AN Surlyn + waterglass	100 days	J_{SC} increased and V_{OC} decreased for the first 20 days. The efficiency is constant for 100 days.
EPFL [150]	N3	AM1.5 (1000 W m^{-2}), UV cutoff, 35°C	KI, I_2 in GN	7000 h	J_{SC} increased by 20–30% during the first 1000 h, thereafter reaching a plateau value.
ECN, Solaronix [156]	N3	Fluorescent lamp (1000 W m^{-2}), UV cutoff, 35°C	KI, I_2 in GN Surlyn 1702	9600 h	J_{SC} increased and V_{OC} decreased for the first 2000 h. Passed charge: 103 680 C cm^{-2}.
ECN, INAP, Solaronix [158]	N3	Sulphur lamp (2–3 sun), UV cutoff, 20°C, $\eta = 2\%$	HMImI, LiI, I_2, TBP in MPN Surlyn	8300 h	V_{OC} decreased (50 mV) and J_{SC} increased.
ECN, INAP, Solaronix [158]	N3	UV (10 mW cm^{-2}), 20°C	HMImI, MgI_2, I_2, TBP in AN Surlyn	1500 h	J_{SC} and V_{OC} were constant.
INAP [154]	N3	Sulphur lamp (2.5 sun) UV cutoff, 17°C	LiI, I_2, TBP in MPN	10 000 h	J_{SC} was constant after initial decrease.
NIMC-SOC	N3	AM1.5 (1000 W m^{-2}) UV cutoff, 20°C, $\eta = 5\%$	DMPImI, LiI, I_2, TBP in AN, PN, MPN	4500 h	J_{SC} decreased 5% and V_{OC} was constant. 1.3×10^7 turnovers.
NIMC	Mero-cyanine	AM1.5 (1000 W m^{-2}) UV cutoff, 20°C, $\eta = 3\%$	DMPImI, LiI, I_2 in MAN	1500 h	J_{SC} and V_{OC} were constant. 1×10^6 turnovers.

PC: propylene carbonate, NMO: 3-methyl-2-oxazolidinone, TBAI: tetrabutylammonium iodide, AN: acetonitrile, PN: propionitrile, GN: glutaronitrile, MAN: methoxyacetonitrile, MPN: 3-methoxypropionitrile, TBP: tert-butylpyridine, HMImI: 1-hexyl-3-methylimidazolium iodide, DMPImI: 1,2-dimethyl-3-propylimidazolium iodide
SOC: Sumitomo Osaka Cement Co. Ltd

One of the organic dyes, merocyanine dye, also gave good long-term stability in a preliminary test using a sealed cell under continuous AM1.5 irradiation with a 420-nm cutoff filter, although organic dyes are generally considered to be unstable compared to metal complexes. We obtained stability of cell performance for approximately 1500 h, corresponding to a turnover number of more than 10 million (Table 15.3).

These results strongly indicate that the DSSC shows sufficient physical and chemical stability during the period of illumination. Nevertheless, stability tests at high temperatures and high humidity must be carried out for outdoor applications.

15.4.2 Module Fabrication and Other Subjects for Commercialization

The sheet resistance of TCO substrates (i.e. SnO_2) is relatively high, making the DSSCs resistance-limited if they are larger than about 1 cm^2. Increased sheet resistance of the TCO substrate on scale-up of the DSSC leads to loss of efficiency, especially fill factor. Therefore, scale-up of the DSSC using a modular approach has been investigated [168, 169]. A module consists of several interconnected basic cells with two TCO substrates coated with TiO_2 or platinum, including the electrolyte inside. The electrolyte contains iodine and iodide, which dissolve metal materials, dissolved in an organic solvent. Therefore, standard conductors like silver will not work or has to be protected by sealing materials. In addition, for having an organic solvent in such a system, one must seal the system carefully also at the outside. To seal the modules, an inert material, glass frit, even for interconnections has been used [168]. An efficiency of 7% was achieved using a module consisting of 12 interconnected cells with a total area of 112 cm^2 (7.6% for a 3-cm^2 cell and 8% for a 1-cm^2 cell) [168]. A continuous process for the fabrication of a monolithic series connecting DSSC modules using laser scribing has been proposed by Kay and Grätzel (Figure 15.16) [13].

Recently, polymer substrates instead of glass have been utilized in constructing DSSCs, expanding possible commercial applications [170–174]. Polymer substrates allow roll-to-roll production, which can achieve high throughput. When a polymer film is used as a substrate, aqueous TiO_2 paste without organic surfactants is sintered at relatively low temperatures, approximately 150°C being sufficient to produce mechanically stable TiO_2 films. Sommeling *et al*. at ECN used an ITO-coated poly(ethylene terephthalate) (PET) film as a substrate and prepared a plastic DSSC [170–172]. A cell performance with a J_{SC} of 15 $\mu A\,cm^{-2}$, V_{OC} of 0.48 V, and *ff* of 0.67 was obtained at an illumination intensity of 250 lux. This performance is sufficient to power indoor appliances such as watches and calculators. Under AM1.5 irradiation, a V_{OC} of 0.7 V and J_{SC} of 2 $mA\,cm^{-2}$ were obtained.

Recently, the DSSC has been used for educational demonstration of solar energy–to–electricity conversion because of its simple fabrication [15, 175]. One can purchase DSSC kits including all components, TCO-coated glass, TiO_2 electrodes, blackberries (i.e. dye), and electrolyte solution [176, 177] and easily demonstrate an artificial photosynthetic process. For detailed studies, one can purchase other materials, including Ru complex photosensitizers, TiO_2 paste, and sealing materials from Solaronix S. A. [178].

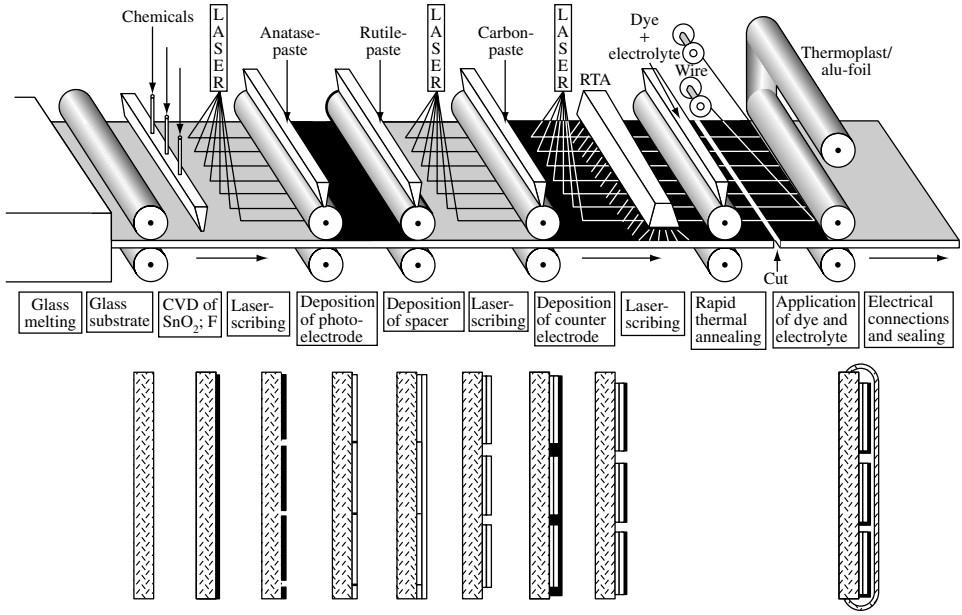

Figure 15.16 Continuous process for the fabrication of monolithic series-connected DSSC modules. Reprinted from *Sol. Energy Mater. Sol. Cells*, **44**, Kay A, Grätzel M, 99–117, © (2002), with permission from Elsevier Science

15.5 SUMMARY AND PROSPECTS

Since 1991, when Grätzel and coworkers reported the development of the highly efficient, novel DSSCs, researchers throughout the world have intensively investigated DSSC mechanisms, new materials, and commercialization. A maximum efficiency of 10.4% has been obtained under AM1.5 in the laboratory. In addition, satisfactory long-term stability of sealed cells has been achieved under relatively mild test conditions (low temperatures and no UV exposure). It will be possible to achieve commercial DSSC production in the near future for indoor applications, such as calculators and several kind of watches. For expanded commercial applications, however, there are several problems that confront us. Overcoming these problems greatly brings DSSC close to expanded commercialization.

(a) Improvement of efficiency

For commercial applications, efficiency higher than 10% (e.g. 15%) is sure to be desired. Expanding the absorption property of the photosensitizer to near IR region is necessary for improved J_{SC}. The absorption property of black dye, whose absorption threshold is close to 920 nm, is expected to be the optimal threshold for single-junction solar cells similar to GaAs. Development of new photosensitizers able to absorb in the near IR region is also desired. Extending of the region of ICPE spectral sensitivity with black dye or other new photosensitizers from the typical 500–600 nm out to 700–900 nm would increase J_{SC} from 20 to 28 mA cm^{-2} resulting in an overall efficiency of 15%. The absorption coefficient of the photosensitizers and the light-scattering effect of the

semiconductor film (described in Section 15.2.2) would improve the IPCE performance in the long-wavelength region. In addition, the energy gaps, ΔE_1 and ΔE_2, as the driving forces for electron-transfer processes (Figure 15.6) are sure to result in energy loss. If we can construct good systems performing with smaller ΔE_1 and ΔE_2 because of molecular design of the photosensitizers, the efficiency can be improved. Improvement of V_{OC} is also important for achievement of higher efficiencies. As shown above, decreased V_{OC} is mainly attributed to recombination between the injected electrons and the redox mediator, I_3^- (dark current). Molecular design of the photosensitizers and/or blocking effect of dark current using adsorbate, such as TBP would improve the V_{OC}. Development of new semiconductor materials, whose conduction-band level is more negative than that of TiO_2, and the new redox mediator, whose redox potential is more positive than that of the I^-/I_3^- redox, would also increase V_{OC} of DSSC. Presently, however, good semiconductor materials and redox mediators exceeding the combination between the TiO_2 electrode and the iodine redox have not been found.

(b) Long-term stability for outdoor applications

As shown in Section 15.4.1.2, satisfactory long-term stability of sealed cells has already been achieved under relatively mild testing conditions (low temperatures and no UV exposure). For outdoor applications, additional stability testing under more rigorous conditions will be required (e.g. high temperature at near 80°C, high humidity, and UV exposure).

(c) Solid electrolyte

As shown in Section 15.3.4, development of solid-state electrolytes in DSSCs is essential for developing a cell with long-term stability and is critical for commercialization. Several organic and inorganic materials, such as OMeTAD, polypyrrole, CuSCN, and CuI, have been investigated as solid electrolytes. Presently, however, performance of solid-state DSSCs using these materials are inferior to that of DSSC using liquid electrolytes. It is very difficult to form a good solid–solid interface, which will produce a high solar cell performance because of the large surface area of the nanoporous TiO_2 electrode. On the other hand, liquid electrolytes can easily penetrate into the nanoporous TiO_2 electrode. One of the factors determining high performance of DSSC is the easy formation of solid–liquid interface between the nanoporous TiO_2 electrode and liquid electrolyte. Therefore, electron-transfer processes can occur at most part of the interface. Low electron (or hole) conductivity of the solid electrolyte materials would also determine low performance of solid-state DSSC. CuI is one of the more attractive materials used for solid electrolyte in DSSC and 4% efficiency was attained using TiO_2/dye/CuI system, as shown in Section 15.3.4. For commercial applications, improvement of the cell performance and long-stability testing of the cell are required because long term stability of the CuI system has not been clarified. Development of new solid electrolyte materials is also desired.

REFERENCES

1. Gerischer H, Tributsch H, *Ber. Bunsen-Ges. Phys. Chem.* **72**, 437–445 (1968).
2. Tributsch H, Gerischer H, *Ber. Bunsen-Ges. Phys. Chem.* **73**, 251–260 (1969).
3. Anderson S *et al*., *Nature* **280**, 571–573 (1979).

4. Dare-Edwards M *et al*., *Faraday Discuss. Chem. Soc.* **70**, 285–298 (1980).
5. O'Regan B, Grätzel M, *Nature* **353**, 737–740 (1991).
6. Nazeeruddin Md *et al*., *J. Am. Chem. Soc.* **115**, 6382–6390 (1993).
7. Nazeeruddin Md, Péchy P, Grätzel M, *Chem. Commun.* 1705–1706 (1997).
8. Nazeeruddin Md, *J. Am. Chem. Soc.* **123**, 1613–1624 (2001).
9. Kalyanasundaram K, Grätzel M, "Metal Complexes as Photosensitizers in Photoelectrochemical Cells", in Kalyanasundaram K, Grätzel M, Eds, *Photosensitization and Photocatalysis Using Inorganic and Organometallic Compounds*, 247–271, Kluwer Academic Publishers, Dordrecht, Netherlands (1993).
10. Smestad G, Bignozzi C, Argazzi R, *Sol. Energy Mater. Sol. Cells* **32**, 259–273 (1994).
11. Smestad G, *Sol. Energy Mater. Sol. Cells* **32**, 259–288 (1994).
12. Hagfeldt A, Grätzel M, *Chem. Rev.* **95**, 49–68 (1995).
13. Kay A, Grätzel M, *Sol. Energy Mater. Sol. Cells* **44**, 99–117 (1996).
14. Bignozzi C, Schoonover J, Scandola F, "A Supramolecular Approach to Light Harvesting and Sensitization of Wide-Bandgap Semiconductors: Antenna Effects and Charge Separation", in Meyer G, Ed, *Molecular Level Artificial Photosynthetic Materials*, 1–97, John Wiley & Sons, New York, NY (1997).
15. Smestad G, *Sol. Energy Mater. Sol. Cells* **55**, 157–178 (1998).
16. Kalyanasundaram K, Grätzel M, *Coord. Chem. Rev.* **77**, 347–414 (1998).
17. Grätzel M, *Curr. Opin. Colloid Interface Sci.* **4**, 314–321 (1999).
18. Hagfeldt A, Grätzel M, *Acc. Chem. Res.* **33**, 269–277 (2000).
19. Argazzi R *et al*., *Inorg. Chem.* **33**, 5741–5749 (1994).
20. Finnie K, Bartlett J, Woolfrey J, *Langmuir* **14**, 2744–2749 (1998).
21. Nazeeruddin Md *et al*., *Langmuir* **16**, 8525–8528 (2000).
22. Murakoshi K *et al*., *J. Electroanal. Chem.* **396**, 27–34 (1995).
23. Sayama K, Sugihara H, Arakawa H, *Chem. Mater.* **10**, 3825–3832 (1998).
24. Liu Y, Hagfeldt A, Xiao X, Lindquist S, *Sol. Energy Mater. Sol. Cells* **55**, 267–281 (1998).
25. Hara K *et al*., *Sol. Energy Mater. Sol. Cells* **70**, 151–161 (2001).
26. Vlachopoulos N, Liska P, Augustynski J, Grätzel M, *J. Am. Chem. Soc.* **110**, 1216–1220 (1988).
27. Zaban A, Ferrere S, Gregg B, *J. Phys. Chem. B* **102**, 452–460 (1998).
28. Tachibana Y *et al*., *J. Phys. Chem.* **100**, 20056–20062 (1996).
29. Rehm J *et al*., *J. Phys. Chem.* **100**, 9577–9578 (1996).
30. Kamat P, Bedja I, Hotchandani S, Patterson L, *J. Phys. Chem.* **100**, 4900–4908 (1996).
31. Nasr C, Liu D, Hotchandani S, Kamat P, *J. Phys. Chem.* **100**, 11054–11061 (1996).
32. Hannappel T, Burfeindt B, Storck W, Willig F, *J. Phys. Chem. B* **101**, 6799–6802 (1997).
33. Heimer T, Heilweil E, *J. Phys. Chem. B* **101**, 10990–10993 (1997).
34. Cherepy N, Smestad G, Grätzel M, Zhang J, *J. Phys. Chem. B* **101**, 9342–9351 (1997).
35. Murakoshi K, Yanagida S, Capel M, Castner Jr. E, in Moskovits M, Ed, *Interfacial Electron Transfer Dynamics of Photosensitized Zinc Oxide Nanoclusters*, 221–238, American Chemical Society, Washington, DC (1997).
36. Ellingson R *et al*., *J. Phys. Chem. B* **102**, 6455–6458 (1998).
37. Asbury J, Wang Y, Lian T, *J. Phys. Chem. B* **103**, 6643–6647 (1999).
38. Heimer T, Heilweil E, Bignozzi C, Meyer G, *J. Phys. Chem. A* **104**, 4256–4262 (2000).
39. Tachibana Y *et al*., *J. Phys. Chem. B* **104**, 1198–1205 (2000).
40. Huber R *et al*., *J. Phys. Chem. B* **104**, 8995–9003 (2000).
41. Iwai S *et al*., *J. Chem. Phys.* **113**, 3366–3373 (2000).
42. Willig F, "Dye-Sensitized Electron Injection into Semiconductor Electrodes", in Miller R *et al*., Eds, *Surface Electron Transfer Processes*, 167–309, VCH Publishers, New York (1995).
43. Moser J, Grätzel M, *Chimia* **52**, 160–162 (1998).
44. Asbury J, Hao E, Wang Y, Lian T, *J. Phys. Chem. B* **104**, 11957–11964 (2000).
45. Asbury J *et al*., *J. Phys. Chem. B* **105**, 4545–4557 (2001).

46. Benkö G *et al*., *J. Am. Chem. Soc.* **124**, 489–493 (2002).
47. Huber R, Moser J, Grätzel M, Wachtveitl J, *J. Phys. Chem. B* **106**, 6494–6499 (2002).
48. Haque S, Tachibana Y, Klug D, Durrant J, *J. Phys. Chem. B* **102**, 1745–1749 (1998).
49. Haque S *et al*., *J. Phys. Chem. B* **104**, 538–547 (2000).
50. Kuciauskas D *et al*., *J. Phys. Chem. B* **105**, 392–403 (2001).
51. Nasr S, Hotchandani S, Kamat P, *J. Phys. Chem. B* **102**, 4944–4951 (1998).
52. Huang S *et al*., *J. Phys. Chem. B* **101**, 2576–2582 (1997).
53. Kumar A, Santangelo P, Lewis N, *J. Phys. Chem.* **96**, 834–842 (1992).
54. Stanley A, Matthews D, *Aust. J. Chem.* **48**, 1293–1300 (1995).
55. Matthews D, Infelta P, Grätzel M, *Sol. Energy Mater. Sol. Cells* **44**, 119–155 (1996).
56. Salafsky J, Lubberhuizen W, van Faassen E, Schropp R, *J. Phys. Chem. B* **102**, 766–769 (1998).
57. Duffy N, Peter L, Rajapakse R, Wijayantha K, *J. Phys. Chem. B* **104**, 8916–8919 (2000).
58. Cahen D *et al*., *J. Phys. Chem. B* **104**, 2053–2059 (2000).
59. Gregg B, Pichot F, Ferrere S, Fields C, *J. Phys. Chem. B* **105**, 1422–1429 (2001).
60. Cao F, Oskam G, Meyer G, Searson P, *J. Phys. Chem. B* **100**, 17021–17027 (1996).
61. Solbrand A *et al*., *J. Phys. Chem. B* **101**, 2514–2518 (1997).
62. Solbrand A *et al*., *J. Phys. Chem. B* **103**, 1078–1083 (1999).
63. Sommeling P *et al*., *Sol. Energy Mater. Sol. Cells* **62**, 399–410 (2000).
64. Hoyer P, Weller H, *J. Phys. Chem. B* **99**, 14096–14100 (1995).
65. Schwarzburg K, Willig F, *Appl. Phys. Lett.* **58**, 2520–2522 (1991).
66. de Jongh P, Vanmaekelbergh D, *Phys. Rev. Lett.* **77**, 3427–3430 (1996).
67. de Jongh P, Vanmaekelbergh D, *J. Phys. Chem. B* **101**, 2716–2722 (1997).
68. Könenkamp R, Henniger R, Hoyer P, *J. Phys. Chem.* **97**, 7328–7330 (1993).
69. Wahl A, Augustynski J, *J. Phys. Chem. B* **102**, 7820–7828 (1998).
70. Nelson J, *Phys. Rev. B* **59**, 15374–15380 (1998).
71. van de Lagemaat J, Park N, Frank A, *J. Phys. Chem. B* **104**, 2044–2052 (2000).
72. Kopidakis N *et al*., *J. Phys. Chem. B* **104**, 3930–3936 (2000).
73. van de Lagemaat J, Frank A, *J. Phys. Chem. B* **104**, 4292–4294 (2000).
74. Kambe S *et al*., *J. Phys. Chem. B* **106**, 2967–2972 (2002).
75. 2-24-15 Aoyama, Minato-ku, Tokyo 107, Japan, FAX: +81-3-402-4289.
76. Barbé C *et al*., *J. Am. Ceram. Soc.* **80**, 3157–3171 (1997).
77. Park N, van de Lagemaat J, Frank A, *J. Phys. Chem. B* **104**, 8989–8994 (2000).
78. 53 Church Hill Road, Newton, CT 06470-1614, USA, FAX: 203-270-4610, E-mail: info@sonicsandmaterials.com.
79. Usami A, *Chem. Phys. Lett.* **277**, 105–108 (1997).
80. Ferber J, Luther J, *Sol. Energy Mater. Sol. Cells* **54**, 265–275 (1998).
81. Rothenberger G, Comte P, Grätzel M, *Sol. Energy Mater. Sol. Cells* **58**, 321–336 (1999).
82. Tachibana Y, Hara K, Sayama K, Arakawa H, *Chem. Mater.* **14**, 2527–2535 (2002).
83. Bonhôte P *et al*., *Inorg. Chem.* **35**, 1168–1178 (1996).
84. Papageorgiou N *et al*., *J. Electrochem. Soc.* **143**, 3099–3108 (1996).
85. Papageorgiou N, Maier W, Grätzel M, *J. Electrochem. Soc.* **144**, 876–884 (1997).
86. Redmond G, Fitzmaurice D, Grätzel M, *Chem. Mater.* **6**, 686–691 (1994).
87. Rensmo H *et al*., *J. Phys. Chem. B* **101**, 2598–2601 (1997).
88. Rao T, Bahadur L, *J. Electrochem. Soc.* **144**, 179–185 (1997).
89. Keis K, Lindgren J, Lindquist S, Hagfeldt A, *Langmuir* **16**, 4688–4694 (2000).
90. Hara K *et al*., *Chem. Lett.* 316–317 (2000).
91. Hara K *et al*., *Sol. Energy Mater. Sol. Cells* **64**, 115–134 (2000).
92. Equchi K, Koga H, Sekizawa K, Sasaki K, *J. Ceram. Soc. Jpn.* **108**, 1067–1071 (2000).
93. Nasr S, Kamat P, Hotchandani S, *J. Phys. Chem. B* **102**, 10047–10056 (1998).
94. Burnside S *et al*., *J. Phys. Chem. B* **103**, 9328–9332 (1999).
95. He J, Lindström H, Hagfeldt A, Lindquist S, *J. Phys. Chem. B* **103**, 8940–8943 (1999).

96. Tennakone K, Kumara G, Kottegoda I, Perera V, *Chem. Commun.* 15–16 (1999).
97. Tennakone K *et al*., *Chem. Mater.* **11**, 2474–2477 (1999).
98. Kay A, Grätzel M, *Chem. Mater.* **14**, 2930–2935 (2002).
99. Zaban A, Chen S, Chappel S, Gregg B, *Chem. Commun.* 2231–2232 (2000).
100. Wang Z *et al*., *Chem. Mater.* **13**, 678–682 (2001).
101. Heimer T, Bignozzi C, Meyer G, *J. Phys. Chem.* **97**, 11987–11994 (1993).
102. Argazzi R *et al*., *Inorg. Chem.* **33**, 5741–5749 (1994).
103. Nazeeruddin M *et al*., *J. Chem. Soc., Dalton Trans.* 4571–4578 (1997).
104. Shklover V *et al*., *Chem. Mater.* **9**, 430–439 (1997).
105. Argazzi R, Bignozzi C, Hasselmann G, Meyer G, *Inorg. Chem.* **37**, 4533–4537 (1998).
106. Liska P *et al*., *J. Am. Chem. Soc.* **110**, 3686–3687 (1998).
107. Shklover V *et al*., *Chem. Mater.* **10**, 2533–2541 (1998).
108. Ruile S, Kohle O, Pettersson H, Grätzel M, *New J. Chem.* 25–31 (1998).
109. Zakeeruddin S, Nazeeruddiin Md, Humphry-Baker R, Grätzel M, *Inorg. Chem.* **37**, 5251–5259 (1998).
110. Jing B *et al*., *J. Mater. Chem.* **8**, 2055–2060 (1998).
111. Sugihara H *et al*., *Chem. Lett.* 1005–1006 (1998).
112. Lees A *et al*., *Eur. J. Inorg. Chem.* 2309–2317 (1999).
113. Thompson D, Kelly C, Farzad F, Meyer G, *Langmuir* **15**, 650–653 (1999).
114. Islam A *et al*., *Chem. Lett.* 490–491 (2000).
115. Yanagida M *et al*., *J. Chem. Soc., Dalton Trans.* 2817–2822 (2000).
116. Schwarz O *et al*., *J. Photochem. Photobiol., A: Chem.* **132**, 91–98 (2000).
117. Hara K *et al*., *Langmuir* **17**, 5992–5999 (2001).
118. Takahashi Y *et al*., *Inorg. Chim. Acta* **310**, 169–174 (2000).
119. Aranyos V *et al*., *Sol. Energy Mater. Sol. Cells* **64**, 97–114 (2000).
120. Renouard T *et al*., *Inorg. Chem.* **41**, 367–378 (2002).
121. Yanagida M *et al*., *New J. Chem.* **26**, 963–965 (2002).
122. Islam A *et al*., *New J. Chem.* **26**, 966–968 (2002).
123. Ferrere S, Gregg B, *J. Am. Chem. Soc.* **120**, 843–844 (1998).
124. Yang M, Thompson D, Meyer G, *Inorg. Chem.* **39**, 3738–3739 (2000).
125. Alebbi M *et al*., *J. Phys. Chem. B* **102**, 7577–7581 (1998).
126. Trammell S, Meyer T, *J. Phys. Chem. B* **103**, 104–107 (1999).
127. Sauvé G *et al*., *J. Phys. Chem. B* **104**, 3488–3491 (2000).
128. Sauvé G *et al*., *J. Phys. Chem. B* **104**, 6821–6836 (2000).
129. Hasselmann G, Meyer G, *Z. Phys. Chem.* **212**, 39–44 (1999).
130. Islam A *et al*., *New J. Chem.* **24**, 343–345 (2000).
131. Kay A, Grätzel M, *J. Phys. Chem.* **97**, 6272–6277 (1993).
132. Kay A, Humphry-Baker R, Grätzel M, *J. Phys. Chem.* **98**, 952–959 (1994).
133. Boschloo G, Goossens A, *J. Phys. Chem.* **100**, 19489–19494 (1996).
134. Tennakone K *et al*., *J. Photochem. Photobiol., A: Chem.* **108**, 175–177 (1997).
135. Nazeeruddin Md, Humphry-Baker R, Grätzel M, Murrer B, *Chem. Commun.* 719–720 (1998).
136. Ferrere S, Zaban A, Gregg B, *J. Phys. Chem.* **101**, 4490–4493 (1997).
137. Sayama K *et al*., *Chem. Lett.* 753–754 (1998).
138. Khazraji A, Hotchandani S, Das S, Kamat P, *J. Phys. Chem. B* **103**, 4693–4700 (1999).
139. Wang Z, Li F, Huang C, *Chem. Commun.* 2063–2064 (2000).
140. Wang Z *et al*., *J. Phys. Chem. B* **104**, 9676–9682 (2000).
141. Sayama K *et al*., *Chem. Commun.* 1173–1174 (2000).
142. Sayama K *et al*., *New J. Chem.* **25**, 200–202 (2001).
143. Hara K *et al*., *Chem. Commun.* 569–570 (2001).
144. Gao F, Bard A, Kispert L, *J. Photochem. Photobiol., A: Chem.* **130**, 49–56 (2000).
145. Hara K *et al*., *J. Phys. Chem. B* **107**, 597–606 (2003).
146. Tennakone K *et al*., *J. Photochem. Photobiol., A: Chem.* **108**, 193–195 (1997).

147. Tennakone K *et al*., *J. Photochem. Photobiol., A: Chem.* **117**, 137–142 (1998).
148. Matsumoto H *et al*., *Chem. Lett.* 26–27 (2001).
149. Bach U *et al*., *Nature* **395**, 583–585 (1998).
150. Bach U *et al*., *J. Am. Chem. Soc.* **121**, 7445–7446 (1999).
151. Tennakone K *et al*., *J. Phys. D: Appl. Phys.* **31**, 1492–1496 (1998).
152. Tennakone K, Perera U, Kottegoda I, Kumara G, *J. Phys. D: Appl. Phys.* **32**, 374–379 (1999).
153. O'Regan B, Schwartz D, *J. Appl. Phys.* **80**, 4749–4754 (1996).
154. Kumara G *et al*., *Sol. Energy Mater. Sol. Cells* **69**, 195–199 (2001).
155. Murakoshi K, Kogure R, Wada Y, Yanagida S, *Sol. Energy Mater. Sol. Cells* **55**, 113–125 (1998).
156. Kubo W *et al*., *Chem. Lett.* 1241–1242 (1998).
157. Mikoshiba S, Sumino H, Yonetsu M, Hayase S, *Proc. 16th European Photovoltaic Solar Energy Conference* (2000).
158. Mikoshiba S, Sumino H, Yonetsu M, Hayase S, Japan Patent, 2001-160427 (2001).
159. Kohle O, Grätzel M, Meyer A, Meyer T, *Adv. Mater.* **9**, 904–906 (1997).
160. Durham B, Casper J, Nagle J, Meyer T, *J. Am. Chem. Soc.* **104**, 4803–4810 (1982).
161. Amirnasr M, Nazeeruddin Md, Grätzel M, *Thermochim. Acta* **348**, 105–114 (2000).
162. Grünwald R, Tributsch H, *J. Phys. Chem. B* **101**, 2564–2575 (1997).
163. Kern R *et al*., *Opto-Electron. Rev.* **8**, 284–288 (2000).
164. Olsen E, Hagen G, Lindquist S, *Sol. Energy Mater. Sol. Cells* **63**, 267–273 (2000).
165. Späth M *et al*., *Proc. 14th European Photovoltaic Solar Energy Conference* (1997).
166. Rijnberg E *et al*., *Proc. 2nd World Conference and Exhibition on Photovoltaic Solar Energy Conversion* (1998).
167. Hinsch A *et al*., *Proc. 16th European Photovoltaic Solar Energy Conference* (2000).
168. Hanke K, *Z. Phys. Chem.* **212**, 1–9 (1999).
169. Pettersson H, Gruszecki T, *Sol. Energy Mater. Sol. Cells* **70**, 203–212 (2001).
170. Sommeling P, Späth M, van Roosmalen J, "Dye-Sensitized Nanocrystalline TiO_2 Solar Cells on Flexible Substrates", *Proc. 2nd World Conference and Exhibition on Photovoltaic Solar Energy Conversion* (1998).
171. Sommeling P *et al*., "Flexible Dye-Sensitized Nanocrystalline TiO_2 Solar Cells", *Proc. 16th European Photovoltaic Solar Energy Conference* (2000).
172. Sommeling P, Späth M, Kroon J, van Roosmalen J, "Flexible Dye-Sensitized Nanocrystalline TiO_2 Solar Cells", *Abstract 13th International Conference on Photochemical Conversion and Storage of Solar Energy* (2000).
173. Hagfeldt A, "Research and Development of Dye-Sensitized Solar Cells at the Angstrom Solar Center", *Abstract 4th NIMC International Symposium on Photoreaction Control and Photofunctional Materials* (2001).
174. Lindström H *et al*., *Nano Lett.* **1**, 97–100 (2001).
175. Smestad G, Grätzel M, *J. Chem. Educ.* **75**, 752–756 (1998).
176. *http://www.solideas.com/solrcell/cellkit.html*, Sol ldeas Technology Department, P.O. Box 51038, Pacific Grove, California 93950, USA. E-mail: info@solideas.com.
177. *http://www.nisinoda-electronics.co.jp/*, 7-1-3 Ebie, Fukushima, Osaka, Japan. FAX: +81-6-6451-7836.
178. *http://www.solaronix.ch/*, Solaronix SA, rue de l'Ouriette 129, 1170 Aubonne VD. FAX: +41-21-821-22-89.